ELECTRICAL CONDUCTIVITY AND GAMMA RAY RESPONSE TO CLAY, WATER, AND CHLORIDE CONTENT IN FISSURED SEDIMENTS, TRANS-PECOS, TEXAS

Final Report

prepared by

Jeffrey G. Paine, Richard S. Goldsmith, and Bridget R. Scanlon

Bureau of Economic Geology
Noel Tyler, Director
The University of Texas at Austin
Austin, Texas 78713-8924

for

National Low-Level Radioactive Waste Management Program,
U.S. Department of Energy,
Assistant Secretary for Environmental Management,
under DOE Idaho Operations Office Contract No. DE-AC07-95ID 13223 and Interagency Contract No. 94-0304

June 1995

QAe7759

CONTENTS

Figures

Tables

ABSTRACT

Near-surface conductivity profiles determined using surface and borehole electromagnetic induction instruments were compared with each other and with variations in several important hydrological parameters, including clay content, water content, and chloride content in unsaturated sediments in fissured settings. Time-domain electromagnetic soundings were acquired at 10 boreholes in the Eagle Flat, Red Light Bolson, Hueco Bolson, and Ryan Flat areas in the arid Trans-Pecos region of West Texas. These boreholes were logged with induction and passive radiation probes to determine conductivity profiles and natural gamma ray activity.

At the Red Light Bolson and Hueco Bolson fissures, the gamma logs were sensitive to clay content and followed the conventional trend of increasing count rates with increasing clay content. At Eagle Flat, gamma count rates were not much higher in the clay fraction than they were in the silt and sand fraction; thus the gamma log underestimated the variability in clay content. At the Ryan Flat fissure, gamma count rates were higher than for the other fissure sites and were higher for the sand and silt fraction than for the clay fraction. This suggests that the sedimentary grains making up these deposits are volcanogenic and that the coarse fraction contains a larger percentage of K-bearing minerals than the clay fraction.

Time-domain soundings produced simplified models of subsurface conductivity, successfully detected several abrupt changes in conductivity related to changes in clay or water content, and provided useful conductivity data from below the deepest levels penetrated by the boreholes. Time-domain conductivity profiles are similar to most borehole probe profiles but have far less vertical resolution. Subtle conductivity changes, which can be important in vadose studies, are detected poorly with time-domain methods.

Borehole conductivity profiles correlate best to water and clay content. Chloride content has little influence on conductivity, particularly where water content is low. At the Eagle Flat, Red Light Bolson, and Hueco Bolson fissures, soil conductivity increased with water content

only above a threshold water content. This threshold value depended on soil texture: it was about 0.03 g/g for the relatively fine grained Eagle Flat fissure and was 0.07 g/g at the coarser Red Light Bolson and Hueco Bolson fissures. Perhaps due to the presence of clays with low cation exchange capacities, there was little correlation between water content and soil conductivity at the Ryan Flat fissure.

Borehole gamma and induction logging is an important tool in developing an accurate understanding of vertical variation in texture and conductivity. These logs place discrete samples in better context and can guide sample selection. Differences in gamma response to clay content and the variable relationship of soil conductivity to water, clay, and chloride content at these fissure sites reinforce the importance of sampling.

INTRODUCTION

Soil electrical conductivity responds to several parameters (McNeill, 1980a; Rhoades, 1981) that are important in hydrological investigations. In this study, near-surface conductivity profiles determined using surface and borehole electromagnetic induction instruments were compared with each other and with variations in clay content, water content, and chloride content in unsaturated arid-zone soils in fissured and nonfissured settings.

The purposes of this study were to (1) compare surface and borehole electromagnetic induction methods for determining conductivity profiles, surface methods being desirable because they require no boreholes; (2) determine the reliability of borehole gamma ray logs as a proxy for clay content by comparing gamma response with textural analyses of borehole samples; (3) compare soil conductivity profiles with variations in clay, water, and chloride content to determine the relationship between these parameters and soil conductivity and to examine whether conductivity profiles can be used to map changes in water and chloride content with depth; and (4) examine differences in gamma response (a texture proxy) and conductivity profiles (a proxy for clay, water, or chloride content) both between fissure and near-fissure

sediments and among sediments in different fissured areas in the Trans-Pecos region of West Texas.

Surface and borehole geophysical measurements were compared with borehole sample analyses at four fissured sites in intermontane basins within the Basin and Range physiographic province of Trans-Pecos Texas (fig. 1). Each fissure is found in alluvial sediments that are tens to hundreds of meters thick. The four fissures represent a range of ages of fissures as indicated by width-to-depth ratios that vary from 0.1 to 28. Boreholes were drilled as deep as 26 m at the center of each fissure, 10 m from each fissure, and 50 m from each fissure.

The Eagle Flat fissure (fig. 1) examined in this study is described in Jackson and others (1993). This fissure is 1.2 km long and is clearly delineated by vegetation on aerial photographs and on the ground. It consists of depressions that average 20 m long, 1 m wide, and 0.3 m deep. The large width-to-depth ratio suggests that the fissure is old. Trenches indicate that there is no well-defined fracture beneath the fissure.

The Red Light Bolson fissure (fig. 1) lies at the toe of a dissected alluvial fan (Baumgardner and Scanlon, 1992). The fissure trends between N10°W and N25°W, parallel to topographic contours and to the valley axis. The fissure has been partly filled with sediment and has a width-to-depth ratio of about 5.

At Hueco Bolson (fig. 1), the fissure studied is one of three that have been mapped in the area (Baumgardner and Scanlon, 1992). These fissures are in the Camp Rice Formation, which consists of fairly coarse alluvial sediments. The fissure studied is 140 m long and has width-to-depth ratios of 0.2 to 2. Subsurface fractures extend to a depth of at least 6.2 m. The open fractures are filled with sediment.

The Ryan Flat fissure (fig. 1) formed in 1990 (Baumgardner and Scanlon, 1992). This fissure is 2.2 m deep and 0.7 m wide at its deepest part. Its width-to-depth ratio is 0.1, which is consistent with its young age. It formed near an older fissure that is marked by elongate shallow swales and aligned mesquite bushes.

METHODS

A combination of surface electromagnetic, borehole electromagnetic, and radioactivity methods was used to determine the variation in conductivity and gamma radioactivity with depth in each of the fissured areas. Electromagnetic instruments respond to textural changes as well as soil water content and chemistry changes. The gamma logger responds to textural changes only, allowing a better understanding of textural changes with depth and reducing the ambiguity of the electromagnetic data.

Textural, Water Content, and Chloride Content Analyses

Laboratory methods employed for soil texture, water content, and chloride content analyses of borehole samples are described in detail by Scanlon and Goldsmith (1995). Briefly, particle size analyses were conducted on selected soil samples from different profiles where there were large variations in water content. Carbonate was not dissolved in these samples because some of the rock fragments were carbonate. The greater than 2 mm fraction was determined by sieve analysis, and the percent silt and clay were determined by hydrometer analysis (Gee and Bauder, 1982) at the University of Wisconsin Soils and Physical Geography Laboratory. Gravimetric water content was measured by oven drying the soil samples at 105°C for at least 24 hr. To determine chloride content, double-deionized water was added to the dried soil sample in a 3:1 ratio. Samples were agitated on a reciprocal shaker table for 4 hr. The supernatant was filtered through 0.45-mm filters. Chloride was then analyzed by ion chromatography or by potentiometric titration.

Time-Domain Electromagnetic Induction Soundings

Time-domain, or transient, electromagnetic soundings (Kaufman and Keller, 1983; Spies and Frischknecht, 1991) were acquired at the surface using a Geonics PROTEM 47/S instrument. These soundings were acquired at borehole sites to obtain a conductivity profile that could be

compared with detailed conductivity profiles acquired in boreholes. Time-domain devices measure the decay of a transient secondary electromagnetic field produced by the termination of an alternating primary electromagnetic field. The secondary field strength is measured by the receiving coil at discrete moments in time (or "gates") following transmitter current termination. Secondary field strength at early times gives information on conductivity in the shallow subsurface; field strength at later times is related to conductivity at depth. The computer program TEMIX, by Interpex, was used to construct model conductivity profiles that best fit the observed transient decay for each site.

Time-domain soundings were acquired at 10 boreholes that were logged with induction and gamma ray probes. A square, 5- by 5-m single wire transmitter loop carried an alternating current between 2.0 and 3.0 A. A high-frequency receiver coil with an effective area of 33.4 m^2 was placed 12.5 m from the center of the transmitter loop. At most sites, transient decay periods were long enough to allow two primary transmitter frequencies (285 Hz and 75 Hz) to be used. A short transmitter current turn-off time of 0.32 μs was selected to produce a broad transmitter bandwidth to increase resolution in the shallowest part of the subsurface. Transient field measurements were taken between 7 μs and 0.7 ms for the 285-Hz transmitter frequency and between 48 μs and 2.8 ms for the 75-Hz transmitter frequency. Effective penetration depth was a few tens of meters.

Electromagnetic Induction Logging

The electromagnetic induction method (Parasnis, 1973; McNeill, 1980b; Frischknecht and others, 1991; West and Macnae, 1991) was used to measure soil conductivity adjacent to each logged borehole. Induction logs indicate the conductivity in the subsurface adjacent to the borehole. Induction logging measures conductivity indirectly by creating an alternating electromagnetic field around a transmitting coil. This varying field induces current to flow in the formation, which in turn creates a secondary magnetic field that induces a current to flow in a receiver coil. The strength of the secondary field and the receiver current are proportional to the

conductivity of the formation. Conductivity in the vadose zone is generally a function of water content, water conductivity, pore volume and structure, and ion exchange capacity of clay minerals (McNeill, 1980a; Schlumberger, 1989). Because of their high cation exchange capacity and large surface area per unit volume, clay-rich deposits typically have higher conductivities than do sand-rich deposits (McNeill, 1980a).

Ten dry, uncased boreholes in the study area were logged with the Geonics EM39 induction probe in September 1994 shortly after the boreholes were drilled (table 1). The EM39 has a 50-cm transmitter-receiver coil separation, an operating frequency of 39.2 kHz, and a formation penetration radius of about 1 m. Conductivity measurements were taken at 2.5-cm intervals in the borehole.

Natural Gamma Ray Logging

Nearly all naturally occurring gamma radiation is emitted by an isotope of potassium (K^{40}) and isotopes in the uranium (U^{238}) and thorium (Th^{232}) decay series. Gamma probe response is proportional to weight concentrations of these radioactive isotopes in the logged material and is practically proportional to K_2O content, which is generally higher in clays than in siliceous sands (Schlumberger, 1989).

Natural gamma logging of 10 study area boreholes was completed in September 1994 shortly after borehole drilling (table 1). The boreholes were logged using the Geonics Gamma 39 probe, which uses a thallium-activated sodium iodide detector that is 6.5 cm long. Gamma response, in counts per second, was measured at 2.5-cm intervals in the borehole and integrated over 5 seconds for each measurement.

RESULTS

Eagle Flat

Time-domain electromagnetic soundings were collected at the fissure center, 10 m to the east of the fissure, 30 m east of the fissure, and 30 m west of the fissure (fig. 3). Borehole induction and gamma ray logs were acquired from borehole EFF92 0m at the fissure center and from borehole EFF96 10m, located 10 m east of the fissure.

In general, transient decays at each of the four sounding sites show decreasing apparent resistivity with time (fig. 3). Because the transient propagates downward with time, these data suggest that conductivities increase with depth. Relatively simple two- and three-layer models provide good fits to the observed decays; fitting errors for these fits range from 2.8 to 4.5% (table 2). Each profile shows a resistive layer at the surface underlain by more conductive layers. The most resistive and thinnest surface layer is at the fissure center (fig. 3a).

Superimposing time-domain conductivity models and borehole probe conductivity profiles (fig. 4) indicates that (1) the model has the same general features as the probe profile, but the probe profile has better vertical resolution, (2) actual conductivity as measured by the probe is consistently higher than that indicated by the model, and (3) an increase in conductivity at 6 m depth in the probe profile is shifted slightly deeper in the model profile.

A gamma ray log from borehole EFF92 0m (fig. 4) shows relatively high gamma counts between 1.5 and 3.5 m depth and gradually increasing gamma counts below 9 m depth. This response suggests the presence of a clayey layer near the surface and gradually increasing clay content below 9 m, observations that are corroborated by textural analyses of eight samples from the borehole. The gamma log does not support the presence of a significant coarser layer at 17.5 m depth that is inferred from the borehole sample from the same depth (fig. 4). This sample was probably from a thin, coarser layer that is not representative of the stratigraphic levels above and below it.

At EFF92 0m, the borehole conductivity profile closely follows the water content and chloride content profiles (fig. 4). The conductivity increase at 6 m depth correlates to a large increase in water content at the same depth. Below 6 m, chloride content and conductivity both increase erratically, suggesting that conductivity is increasing in response to increasing chloride at chloride contents above 300 mg/kg and water contents above 0.05 to 0.10 g/g.

The conductivity profile derived from a time-domain sounding 10 m east of the fissure fits the EFF96 10m borehole conductivity profile reasonably well to the deepest level logged (fig. 5). The increase in conductivity modeled at 15 m depth is supported by increasing conductivities below 10 m in the borehole conductivity profile and correlates to an abrupt increase in gamma count rates, and thus clay content, at 14 m. Water and clay contents also increase at this depth.

Water content and chloride content in borehole EFF96 10m samples are highly correlated, making it difficult to distinguish the effects of changes in these parameters on conductivity (fig. 5). The borehole conductivity profile is similar to both water and chloride profiles. In general, the upper 15 m at EFF96 10m is less conductive than the same depth range at the fissure center. The near-surface clayey layer detected in the gamma logs at both boreholes has higher clay content at EFF96 10m, but at other depths the clay contents are similar. Chloride content at EFF96 10m is equal to or greater than that at EFF92 0m, whereas water content at EFF96 10m is equal to or less than that at EFF92 0m. This suggests that both water content and chloride content affect conductivity but that water content is the more significant contributor to conductivity at the Eagle Flat fissure boreholes.

Red Light Bolson

Two sets of soundings and borehole logs were acquired near the Red Light Bolson fissure (fig. 1). Sounding RLB1 was located at borehole RLB 0m at the center of the fissure, and sounding RLB2 was located 50 m east of the fissure at borehole RLB 50m. Gamma and conductivity logs were acquired in both boreholes.

Apparent resistivities for both soundings decrease with time (fig. 6a,b), which suggests increasing conductivities with depth. Three-layer conductivity models fit the observed transients well at both sites (fig. 6a,b and table 2). At sounding RLB1 at the fissure center, two relatively resistive layers are underlain by a more conductive layer at a depth of 16 m. At sounding RLB2 adjacent to the fissure, the conductivity profile is similar but consists of a single resistive layer at the surface that is slightly thicker than the combined thickness of the two resistive layers at the fissure center sounding. The basal conductive layers in each sounding have similar conductivities.

Logged conductivity at fissure center borehole RLB 0m is low and is similar to modeled conductivity only in a general way (fig. 7). A gradual conductivity increase below 11 m on the conductivity log may be modeled by a larger apparent increase at 16 m depth, or alternately the modeled increase at 16 m could be related to an increase in water and clay content near the bottom of the borehole. Gamma response, and thus clay content, generally increases downward; above 12 m, variable count rates suggest interbeds of higher and lower clay content. Below 12 m, count rates and clay content are high and more uniform. Textural analyses of six samples from this borehole corroborate the general trend of increasing clay content but fail to show the interbedding above 12 m.

Gamma response and water content are well correlated at borehole RLB 0m and demonstrate that higher clay content translates to higher water content. These sediments are relatively dry and have little chloride, resulting in low logged conductivities. The slight conductivity increase between 10 and 15 m depth is caused by increasing clay and water content in that interval.

The shallower borehole, RLB 50m at the fissure flank, did not completely penetrate the interbedded zone (fig. 8). Logged conductivities are low and generally match the modeled conductivity in the upper 6 m of the borehole. Gamma response is variable, again suggesting interbedded sediments with differing clay content. The interbedding interpreted from the gamma log is supported by textural analyses of borehole samples. Water content is highly correlated to

gamma count rates; chloride content is higher at the fissure flank than at the fissure center and also correlates to gamma count rates. More-clay-rich interbeds contain more water and chloride than do less-clay-rich units.

Logged conductivity increases downward and follows the general trend of downward increases in clay and water content. Above 2.5 m depth, conductivities, gamma count rates, and water and chloride contents at the fissure flank are similar to those at the fissure center. Below 2.5 m, conductivities are higher at the fissure flank than they are at the fissure center. This effect is caused by higher water and chloride contents at the fissure flank below 2.5 m. Gamma count rates (and clay content) are very similar in the two boreholes to at least 6 m depth.

Hueco Bolson

Three sets of soundings and borehole gamma and conductivity logs were acquired at boreholes near the Hueco Bolson fissure (fig. 1). Sounding HB1 is located at the center of the fissure at borehole HBF 0m, sounding HB2 is located 10 m south of the fissure at borehole HBF 10m, and sounding HB3 is located 50 m south of the fissure at borehole HBF 50m.

Apparent resistivities decrease with time at all three sounding sites, indicating general increases in conductivity with depth (fig. 9a,b,c). Model conductivity profiles at sounding HB1 at the fissure and HB2 10 m from the fissure are similar (fig. 9a,b, table 2) and consist of a surface resistive layer underlain by alternating conductive and resistive layers. The deepest layers begin below 30 m depth and are the most conductive. The conductivity model for sounding HB3, the farthest from the fissure, consists of three layers with conductivities increasing downward.

At borehole HBF 0m at the center of the fissure, logged conductivities are low in the upper 6 m, increase between 6 and 16 m, and are relatively constant between 16 m and the deepest level logged (fig. 10). The top two layers of the time-domain conductivity model form a simplified version of the logged conductivity profile, with good agreement in the upper 6 m and underestimated conductivities at most other logged depths. Gamma response in borehole HBF 0m suggests interbedded layers with more and less clay in the upper 8 m of section and gradually

increasing clay content below 8 m. Textural sample density was not sufficient to show the interbedding in the upper 8 m clearly, but the general trend of increasing clay content downward is apparent.

Above 15 m depth in borehole HBF 0m, logged conductivity most closely follows water content, which in turn is generally correlated to clay content. Chloride content is low in the upper 15 m at this borehole but increases below 15 m and is probably responsible for the slight downward increase in conductivity in a zone where water content is constant or decreasing.

Caving at borehole HBF 10m prevented gamma and conductivity logging below 9 m depth (fig. 11). Logged conductivity in most of this zone is lower than that modeled from time-domain data, but both methods do indicate very low conductivity. The gamma log reveals that there are three high clay content intervals in the upper 9 m of section. Textural analyses in the same depth range are consistent with the gamma log except for the sample at 3 m depth, which should have lower clay content than the sample above it.

The water content profile at borehole HBF 10m closely follows the gamma log, but only slight increases in conductivity are recorded for the two gamma and water content peaks between the surface and 5 m depth. The conductivity log records a larger increase below 7 m, which coincides with the third gamma and water content peak. Chloride content is low throughout the logged section and has little influence on conductivity. Below the deepest level logged, a more conductive zone is modeled between 12 and 23 m depth from time-domain data. This conductive zone roughly correlates to a section that has higher water and chloride content between 14 and 23 m depth. A more resistive zone below 23 m correlates well with an abrupt drop in water content at that level and a gradual drop in chloride content.

Only the uppermost 5 m of borehole HBF 50m could be logged because the borehole caved severely after auger withdrawal (fig. 12). Logged conductivity in the shallow subsurface, like that at borehole HBF 0m, is lower than that modeled from sounding data, but both are very low. Gamma response shows more textural variation than is apparent from textural analyses of borehole samples and suggests the presence of a clay-rich unit between the surface and 2 m depth

and an underlying, less-clay-rich unit to a depth of 4 m. Clay content increases below 4 m. Textural interpretations of gamma response are strengthened by the water content profile, which is well correlated to the gamma log. The slight conductivity increases recorded in the upper 2 m and below 3 m on the conductivity log also correlate to increases in water content. Chloride content rises slightly between 4 and 6 m depth, which contributes to the modest conductivity increase logged at that level.

Chloride contents increase at progressively shallower depths as distance from the fissure increases (figs. 10–12). This zone of increasing chloride content was logged in the fissure center borehole and in the borehole 50 m from the fissure. Both logs show conductivity increases at the depth at which chloride levels increase.

Ryan Flat

Conductivity and gamma logs were acquired in three boreholes near the Ryan Flat fissure (fig. 1). Borehole RFF 0m is located at the center of the fissure, borehole RFF 10m is located 10 m northeast of the fissure, and borehole RFF 50m is located 50 m northeast of the fissure. Time-domain sounding RF1 was acquired at borehole RFF 50m and sounding RF2 was acquired at borehole RFF 10m.

Time-domain soundings 10 m and 50 m distant from the fissure have decreasing apparent conductivities with time, indicating increasing conductivity with depth (fig. 13a,b). Three-layer conductivity models fit the observed data well (fig. 13a,b; table 2) and consist of a relatively resistive surface layer 15 to 20 m thick underlain by two progressively more conductive layers. The deepest boundary modeled is at 40 m in sounding RF1 and at 35 m in sounding RF2. The modeled profile at RF2 is slightly more conductive at all depths than that at the more distant sounding RF1.

Caving at fissure borehole RFF 0m provided less than 5 m of open borehole for logging. Conductivities within this shallow section increase rapidly and are closely correlated to water content, which is generally high in this borehole (fig. 14). The gamma log indicates some

interbedding within the upper 4 m consisting of two high count rate zones between 1 and 2 m depth and at 3 m depth. Textural analyses of borehole samples also show evidence of interbedding in the upper 4 m as well as deeper in the section, but sample density is insufficient to define the vertical textural distribution accurately. Unlike other areas, high count rates are associated with textural samples that have lower clay contents than samples from intervals with higher count rates. Perhaps because of more young volcanic source material in the Ryan Flat area, gamma count rates are higher here than at the Eagle Flat, Red Light Bolson, and Hueco Bolson areas and appear to be higher in the silt and sand size fraction than in the clay fraction.

In the logged interval at fissure borehole RFF 0m, chloride content is quite low and thus is not a significant contributor to conductivity. Water content increases from nearly 0.05 g/g at 1 m depth to more than 0.2 g/g at 3 m depth. This increase is the most likely cause of the downward increase in logged conductivity in borehole RFF 0m.

At borehole RFF 10m, logged conductivity is a little lower than the conductivity modeled from time-domain data for most of the logged section (fig. 15). Borehole conductivity increases gradually to a peak at 10 m depth, then decreases gradually to 14 m depth, the lowest level logged. Time-domain profiles show a conductivity increase below this at 17 m, which may be related to increases in clay and water content at 15 m.

Gamma response in borehole RFF 10m is similar to that at the fissure center borehole for the upper 5 m. Gamma logging deeper into the RFF 10m borehole shows more evidence of interbedding, as do textural analyses of borehole samples. Like at the fissure borehole, many of the textural samples show high clay contents where the gamma log indicates relatively low count rates and low clay contents where the gamma log has high count rates. This relationship is the opposite of that observed at the other fissure sites. Also unlike at other fissure sites, the water content profile and gamma response are inversely correlated. This further suggests that the clay fraction of sediment at Ryan Flat is less radioactive than the silt or sand fraction, probably because the coarser fractions have a significant volcanogenic component.

Above 5 m depth, logged conductivity at RFF 10m is not strongly correlated with either gamma response or water, chloride, or clay content. Below 7 m, conductivity follows the water content profile reasonably well.

Caving also reduced the length of borehole RFF 50m available for logging (fig. 16). This borehole, the farthest of the three from the fissure, has low conductivities near the surface that increase downward to 4 m, the deepest level logged. These logged conductivities are similar to that of layer 1 in the time-domain conductivity model. Although there are few textural analyses of borehole samples in the logged interval, low clay contents correspond to relatively high gamma count rates and high clay contents correspond to relatively low count rates. This again suggests that the silt and sand fraction is more radioactive than the clay fraction at Ryan Flat. The conductivity log of borehole RFF 50m has two minor peaks, which both correlate to relatively low gamma count rates and high water contents.

DISCUSSION

Gamma Response and Clay Content

Most of the fissure sites show the expected trend of increasing gamma counts with increases in clay content (figs. 17a to 20a). Increases in count rates at the Eagle Flat fissure are correlated with increases in clay content (fig. 17a), but occur at a lower rate than at the Red Light Bolson (fig. 18a) and Hueco Bolson (fig. 19a) fissures. Gamma count rates are relatively high at low clay contents at the Eagle Flat fissure, suggesting that the coarse fraction is only slightly less radioactive than the clay fraction at this site. Gamma count rates at the Ryan Flat fissure actually decrease with increasing clay content (fig. 20a). This implies that the sand and silt fraction at Ryan Flat is more radioactive than the clay fraction and that the coarser fractions have more K-bearing minerals than the clay fraction. Higher count rates at this site than at other fissure sites suggest that the sediment grains are younger at Ryan Flat and are probably volcanogenic.

Effects of Clay, Water, and Chloride Content on Conductivity

Increases in clay, water, and chloride content can each increase the conductivity of soil (McNeill, 1980a). Most sediment-forming minerals are quite resistive when dry, but in the presence of water, increasing clay content generally causes an increase in soil conductivity related to increasing pore volume and cation exchange effects. Likewise, pure water is resistive but becomes increasingly electrolytically conductive as its ionic content rises. Borehole conductivity logs and clay, water, and chloride content analyses illustrate the relationship these soil constituents have on conductivity at boreholes near the Eagle Flat, Red Light Bolson, Hueco Bolson, and Ryan Flat fissures (figs. 17b,c,d through 20b,c,d).

At the Eagle Flat fissure borehole (EFF92 0m) and the borehole 10 m east of the fissure (EFF96 10m), there is a wide range of all three constituents and the widest range in observed conductivity among the four fissure sites (fig. 17b,c,d). Water content provides the best relationship to conductivity; water contents above 0.15 g/g are associated with conductivities above 200 mS/m, whereas water contents below 0.05 g/g are associated with conductivities below 100 mS/m. The fissure center borehole and the borehole 10 m from the fissure have similar water content and conductivity trends, but the 10 m borehole is generally drier and less conductive than the fissure borehole. Critical water content, or the water content below which conductivity is not sensitive to changes in water content, is about 0.03 g/g. Clay content is roughly correlated to conductivity, but there are few textural samples, no samples from the borehole 10 m from the fissure, and a large amount of scatter in the few samples that were analyzed from the fissure borehole (fig. 17b). Chloride content and conductivity correlate well in the fissure borehole (fig. 17d), but the 10-m borehole shows consistently lower conductivities at similar chloride contents than does the fissure borehole. This strengthens the argument that water content has the most influence on soil conductivity at the Eagle Flat fissure.

Conductivities are low (less than 75 mS/m) at Red Light Bolson, both in the fissure center borehole RLB 0m and in borehole RLB 50m (50 m from the fissure). Contents of soil

constituents that influence conductivity are also low (fig. 18b,c,d): clay in analyzed samples is below 40 percent, water is below 0.12 g/g, and chloride is below 250 mg/kg. The relatively small conductivity changes observed in these boreholes are most closely correlated to water content changes, but only at water contents above 0.07 g/g (fig. 18c). Below this critical water content, which is higher than that observed in generally finer grained sediments at the Eagle Flat fissure, changes in water content do not produce systematic changes in soil conductivity. Although textural samples have a small range of clay content, samples with higher clay contents have higher conductivities than do those with lower clay contents (fig. 18b). Conductivity does increase with chloride content for the 50 m borehole, but conductivity values vary over an even greater range in the fissure borehole, where chloride content is essentially zero (fig. 18d).

Most of the large range in conductivity measured in three boreholes near Hueco Bolson fissure (fig. 19b,c,d) comes from the fissure borehole, which was deeper than the other two. Conductivity at the Hueco Bolson fissure correlates well with both clay content and water content but not with chloride (fig. 19b,c,d). The relationship between water content and conductivity is similar to that observed at the Red Light Bolson fissure (compare figs. 18c and 19c), where there is a similar range in soil texture. Like at Red Light Bolson, the critical water content at the Hueco Bolson fissure is 0.07 g/g (fig. 19c), higher than that at the Eagle Flat fissure. Above this value, conductivity increases regularly with increases in water content. Chloride content is low at the Hueco Bolson fissure and has little apparent effect on conductivity (fig. 19d).

Data from three boreholes at the Ryan Flat fissure show a wide range in clay and water content, a low to moderate range in chloride content, and unexpectedly low conductivity (fig. 20b,c,d). Taken together, textural data from samples from all three boreholes show that there is a subtle conductivity increase associated with higher clay content (fig. 20b). This relationship is not evident in data from individual boreholes. Conductivity at Ryan Flat also has no strong relationship to water content, despite the wide range of water content values (fig. 20c). Average conductivity for samples with water content higher than 0.15 g/g is only slightly higher than that

for samples with lower water content. Chloride content also appears to have little effect on soil conductivity at the Ryan Flat fissure.

Comparisons of soil texture analyses and water content measurements from Ryan Flat boreholes indicate that water content is higher in clay-rich units than in units with lower clay content and is comparable to water contents at other fissure sites. If clay, water, and chloride contents are similar to those at other fissures with relatively high conductivities, then the markedly lower conductivities at Ryan Flat may be due to the presence of less conductive clay minerals (clays with lower cation exchange capacities, Keller and Frischknecht, 1966). The inverse relationship between clay content and gamma count rates (fig. 20a) also suggests that sediment mineralogy at Ryan Flat is different from that at the other fissure sites.

Utility of Time-Domain Soundings

Determination of subsurface conductivity profiles using time-domain methods is desirable because the method is noninvasive and has potential for greater resolution than can be obtained from most resistivity and frequency-domain techniques. In an attempt to adapt time-domain methods for the shallow subsurface, we used a small transmitter loop, a high-frequency loop current, the shortest available current shut-off time, and a high-frequency receiver with early measurement gates. Nevertheless, the vertical resolution necessary for detailed analysis of changes in water, chloride, and clay content with depth was not obtained. On the positive side, comparisons of time-domain data with borehole data show that the method provided accurate generalized conductivity profiles of the upper few tens of meters at most sites, which allowed overall differences in conductivity profiles to be determined. Additional subsurface features detected with the method included (1) a conductivity increase due to water and chloride content increases at the Eagle Flat fissure (fig. 4), (2) a clay-rich unit with high water and chloride contents adjacent to the Hueco Bolson fissure (fig. 5), (3) abrupt subsurface increases in water and clay contents at the Red Light Bolson fissure (fig. 7), and the top and bottom of a water and chloride content peak at the Hueco Bolson fissure (fig. 11). On the negative side, the method

missed more subtle subsurface conductivity changes that are common at many sites and produced conductivity models that matched actual conductivity profiles only in a general way. For the resolution of the shallow subsurface to improve, broader band transmitters and faster receivers will be required.

CONCLUSIONS

Surface and borehole electromagnetic methods are useful in determining near-surface conductivity, which is responsive to several parameters that are important in vadose-zone hydrological studies. Changes in subsurface conductivity at the Eagle Flat, Red Light Bolson, Hueco Bolson, and Ryan Flat study sites relate to one or more of the following parameters: clay content, water content, and chloride content. In general, increases in any one of these components can produce increases in soil conductivity.

Time-domain electromagnetic soundings produced simplified models of subsurface conductivity, successfully detected several abrupt changes in conductivity related to changes in clay or water content, and provided useful conductivity data from below the deepest levels penetrated by the boreholes. Comparisons of conductivity profiles modeled from time-domain data with those acquired with a borehole electromagnetic probe reveal that the profiles are generally similar, but much detail is lost in the time-domain soundings and most subtle conductivity changes, which are important in vadose studies, are not detected with time-domain methods.

Conductivity profiles determined with a borehole probe at the study sites are mostly a function of water and clay content; chloride content has a relatively minor influence on conductivity, particularly in sections with low water content. At the Eagle Flat, Red Light Bolson, and Hueco Bolson fissure sites, soil conductivity increased with increases in water content only after a critical water content was exceeded. This critical value depended on soil texture—it was about 0.03 g/g for the relatively fine grained Eagle Flat fissure site and was 0.07 g/g at the coarser Red Light Bolson and Hueco Bolson fissure sites. Perhaps because of the

presence of clays with low cation exchange capacities, there was little relationship between water content and soil conductivity at the Ryan Flat fissure despite a wide range of clay and water contents.

At the Red Light Bolson and Hueco Bolson fissures, the gamma logs were a sensitive indicator of clay content and followed the conventional trend of increasing count rates with increasing clay content. At Eagle Flat, gamma count rates were not much higher in the clay fraction than they were in the silt and sand fraction; thus, reliance on the gamma log alone for textural information would have caused the variability in clay content to be underestimated at this site. At the Ryan Flat fissure, gamma count rates were higher than for the other fissure sites and were actually higher for the sand and silt fraction than for the clay fraction. This relationship suggests that the sedimentary grains making up these deposits are volcanogenic and that the coarse fraction contains a larger percentage of K-bearing minerals than the clay fraction.

Borehole gamma and electromagnetic logging is an important tool in developing an accurate understanding of vertical variation in texture and conductivity. These logs place the discrete samples obtained for textural and chemical analyses in a better context and can be a good guide to sample selection. Differences in gamma response to clay content and the relationship of soil conductivity to water, clay, and chloride content at these fissure sites illustrate the continuing importance of borehole sampling for textural and chemical analysis. Proper sampling establishes the relationship between clay content and gamma response and determines whether clay, water, or chloride content variations are the most important cause of soil conductivity changes.

ACKNOWLEDGMENTS

This project was funded by the National Low-Level Radioactive Waste Management Program, U.S. Department of Energy, Assistant Secretary for Environmental Management, under DOE Idaho Operations Office Contract No. DE-AC07-95ID 13233 and Interagency Contract No. 94-0304. The authors gratefully acknowledge the cooperation of the landowners (Deron

Kasparian and El Paso Water Utilities). Word processing was by Susan Lloyd and editing by Bobby Duncan.

REFERENCES

Baumgardner, R. W., Jr., and Scanlon, B. R., 1992, Surface fissures in the Hueco Bolson and adjacent basins, West Texas: The University of Texas at Austin, Bureau of Economic Geology Geological Circular 92-2, 40 p.

Frischknecht, F. C., Labson, V. F., Spies, B. R., Anderson, W. L., 1991, Profiling using small sources, *in* Nabighian, M. N., ed., Electromagnetic methods in applied geophysics—Applications, part A and part B: Tulsa, Oklahoma, Society of Exploration Geophysicists, p. 105–270.

Gee, G. W., and Bauder, J. W., 1982, Particle-size analysis, *in* Page, A.L., ed., Methods of soil analysis, part 2, Chemical and mineralogical methods: Madison, Wisconsin, American Society of Agronomy, p. 383–410.

Jackson, M. L. W., Langford, R. P., and Whitelaw, M. J., 1993, Basin-fill stratigraphy, Quaternary history, and paleomagnetics of the Eagle Flat study area, southern Hudspeth County, Texas: The University of Texas at Austin, Bureau of Economic Geology, report prepared for Texas Low-Level Radioactive Waste Disposal Authority under contract no. IAC(92-93)-0910, 137 p.

Kaufman, A. A., and Keller, G. V., 1983, Frequency and transient soundings: Elsevier, Amsterdam, Methods in Geochemistry and Geophysics, no. 16, 685 p.

Keller, G. V., and Frischknecht, F. C., 1966, Electrical methods in geophysical prospecting: Pergamon Press, New York, 519 p.

McNeill, J. D., 1980a, Electrical conductivity of soils and rocks: Geonics Limited, Mississauga, Ontario, Technical Note TN-5, 22 p.

McNeill, J. D., 1980b, Electromagnetic terrain conductivity measurement at low induction numbers: Geonics Limited, Mississauga, Ontario, Technical Note TN-6, 15 p.

Parasnis, D. S., 1973, Mining geophysics: Amsterdam, Elsevier, 395 p.

Rhoades, J. D., 1981, Predicting bulk soil electrical conductivity versus saturation paste extract electrical conductivity calibrations from soil properties: Soil Science Society of America Journal, v. 45, p. 42–44.

Scanlon, B. R., and Goldsmith, R. S., 1995, Evaluation of subsurface flow in fissured sediments in the Chihuahuan Desert, Texas: The University of Texas at Austin, Bureau of Economic Geology, final report prepared for the National Low-Level Radioactive Waste Management Program, U.S. Department of Energy, Assistant Secretary for Environmental Management, under DOE Idaho Operations Office Contract No. DE-AC07-95ID 13223 and Interagency Contract No. 94-0304, 60 p.

Schlumberger, 1989, Log interpretation principles/applications: Houston, Schlumberger Educational Services, 228 p.

Spies, B. R., and Frischknecht, F. C., 1991, Electromagnetic sounding, *in* Nabighian, M. N., ed., Electromagnetic methods in applied geophysics—Applications, part A and part B: Tulsa, Oklahoma, Society of Exploration Geophysicists, p. 285–386.

West, G. F., and Macnae, J. C., 1991, Physics of the electromagnetic induction exploration method, *in* Nabighian, M. N., ed., Electromagnetic methods in applied geophysics—Applications, part A and part B: Tulsa, Oklahoma, Society of Exploration Geophysicists, p. 5-45.

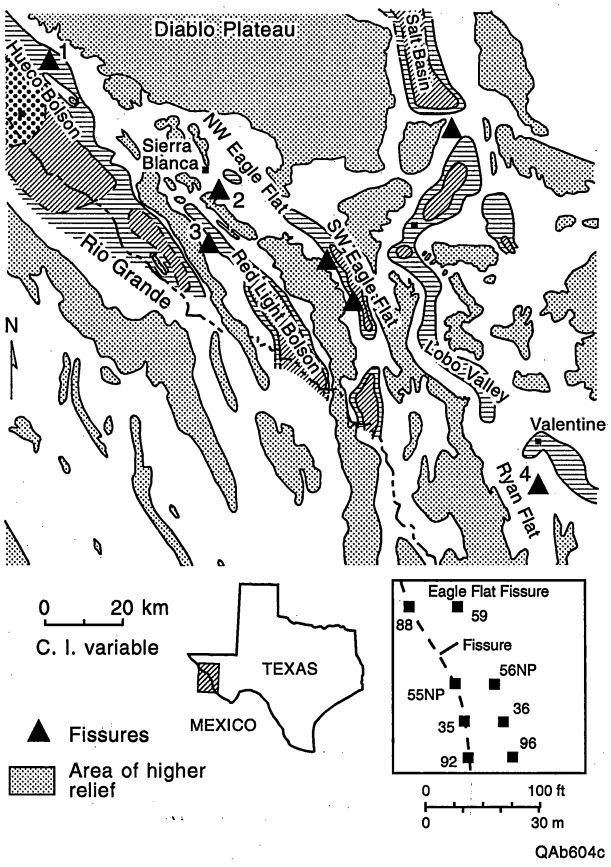

Figure 1. Location of the Eagle Flat, Red Light Bolson, Hueco Bolson, and Ryan Flat fissure areas.

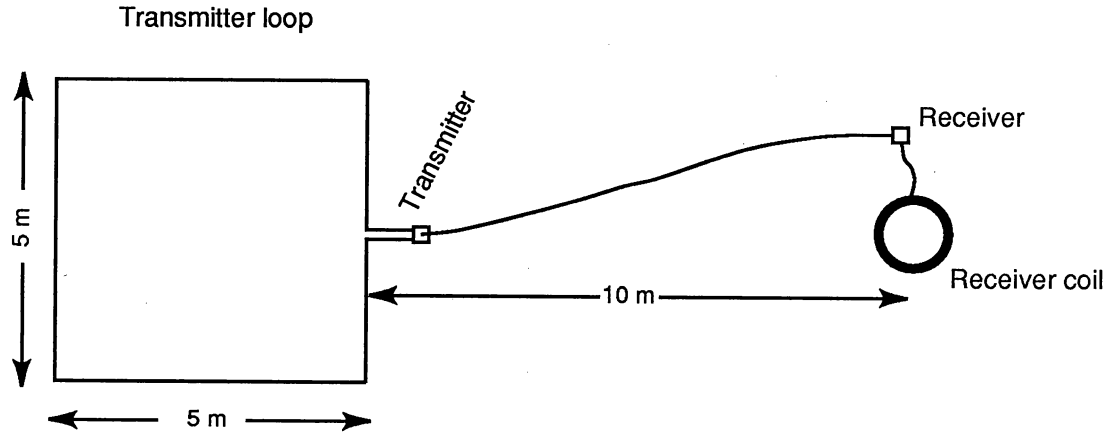

Figure 2. Instrument configuration for PROTEM 47/S sounding.

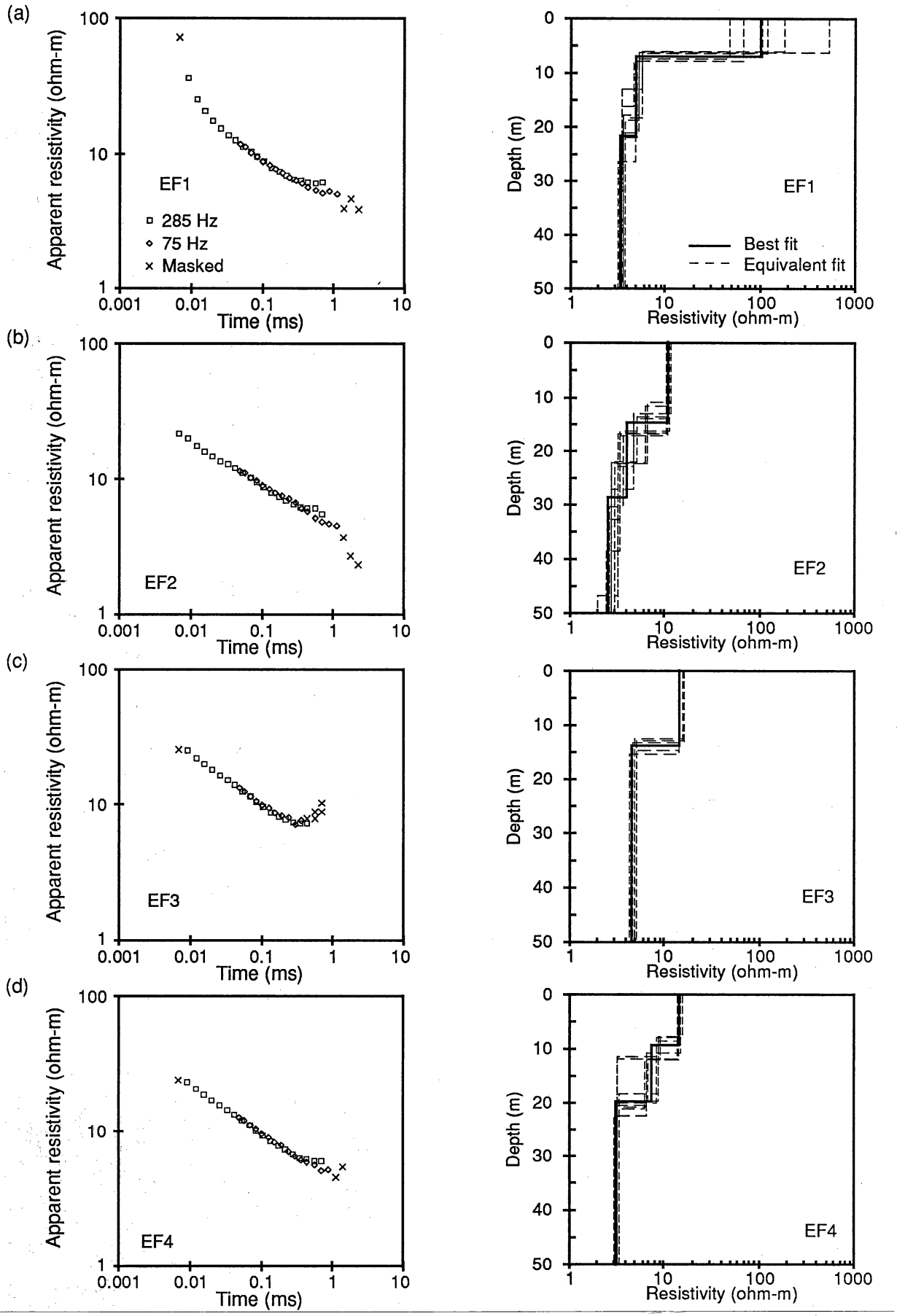

Figure 3. Transient decays (left) and best-fit vertical resistivity models (right) for time-domain soundings at the Eagle Flat fissure. Sounding EF1 (a) is located at borehole EFF92 0m at the center of the fissure, sounding EF2 (b) is located 10 m east of the fissure at borehole EFF96 10m, sounding EF3 (c) is located 30 m east of the fissure, and sounding EF4 (d) is located 30 m west of the fissure. Location shown in fig. 1.

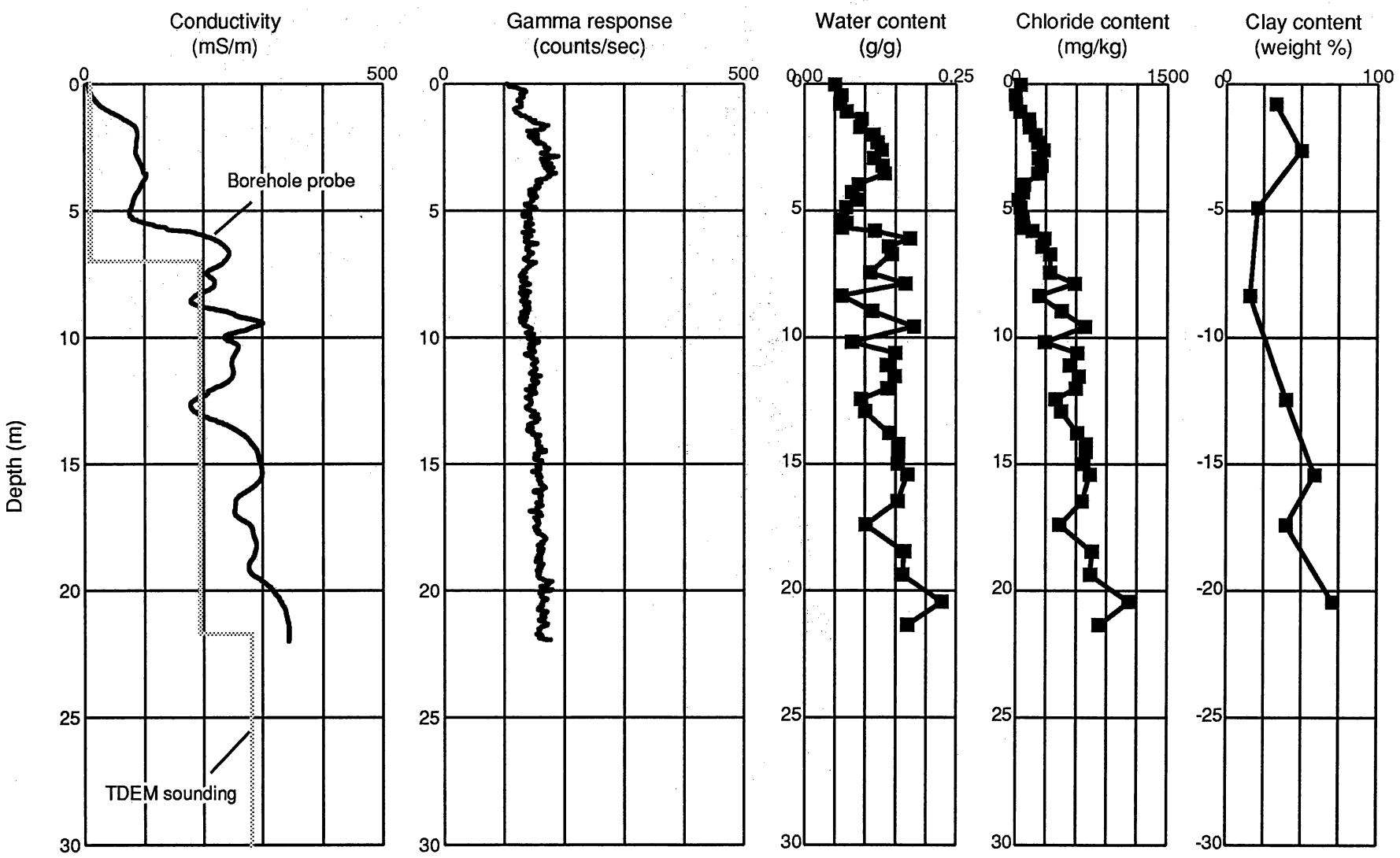

Figure 4. Conductivity, gamma response, soil water content (per gram of sample), chloride content (per kilogram of sample), and clay content for borehole EFF92 0m at the Eagle Flat fissure.

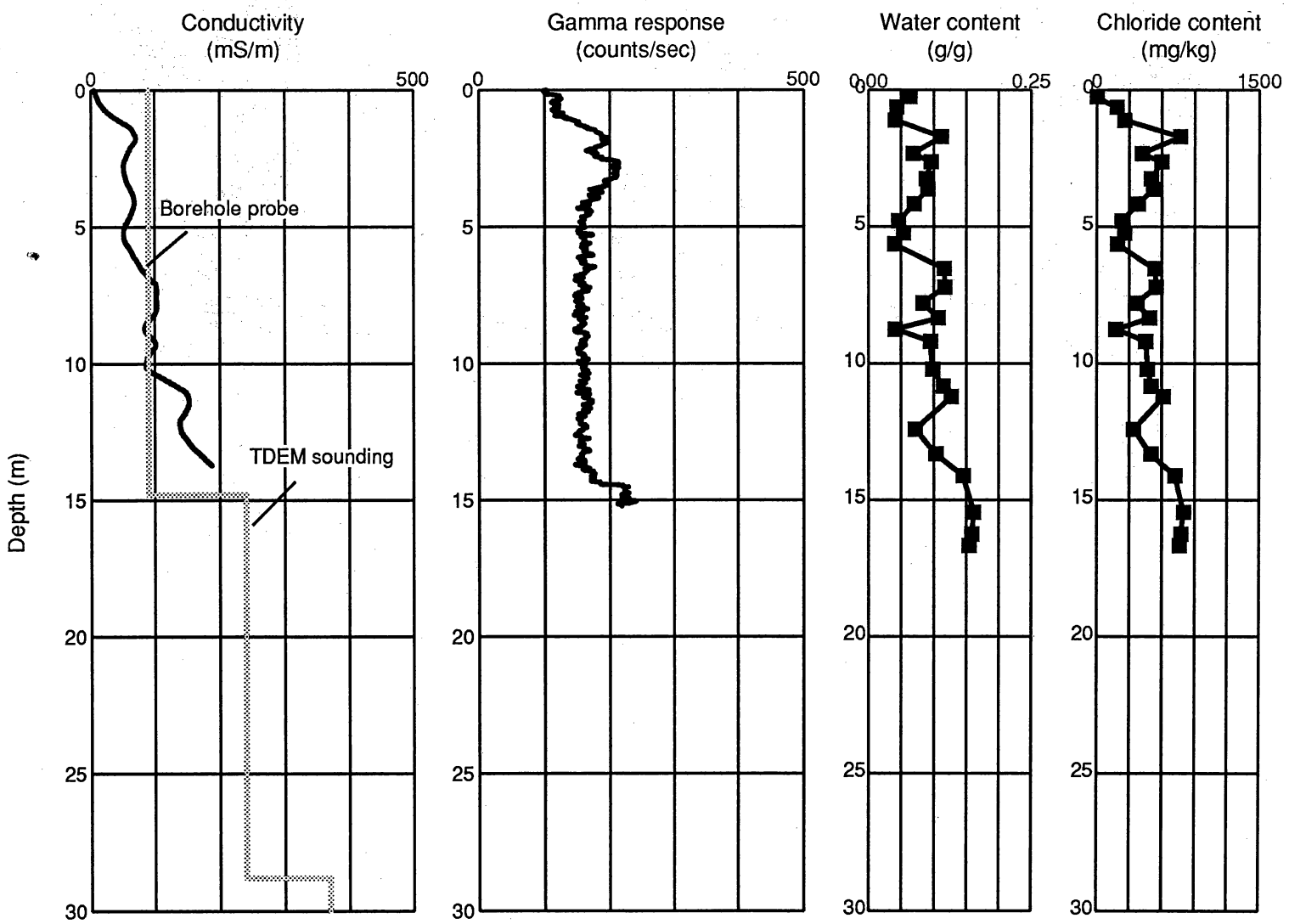

Figure 5. Conductivity, gamma response, soil water content (per gram of sample), and chloride content (per kilogram of sample) for borehole EFF96 10m at the Eagle Flat fissure.

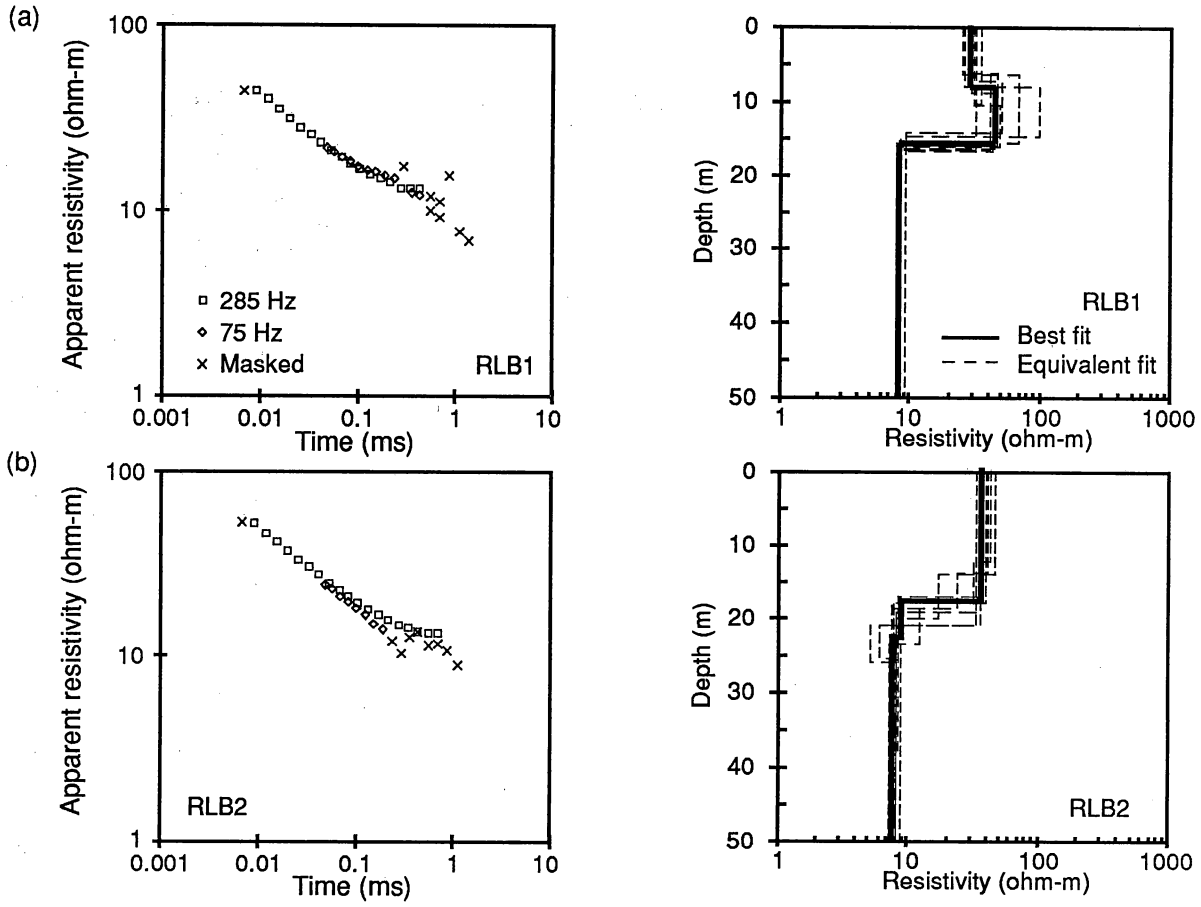

Figure 6. Transient decays (left) and best-fit vertical resistivity models (right) for time-domain soundings at the Red Light Bolson fissure. Sounding RLB1 (a) is located at borehole RLB 0m at the center of a fissure and sounding RLB2 (b) is located 50 m east of the fissure at borehole RLB 50m. Location shown in fig. 1.

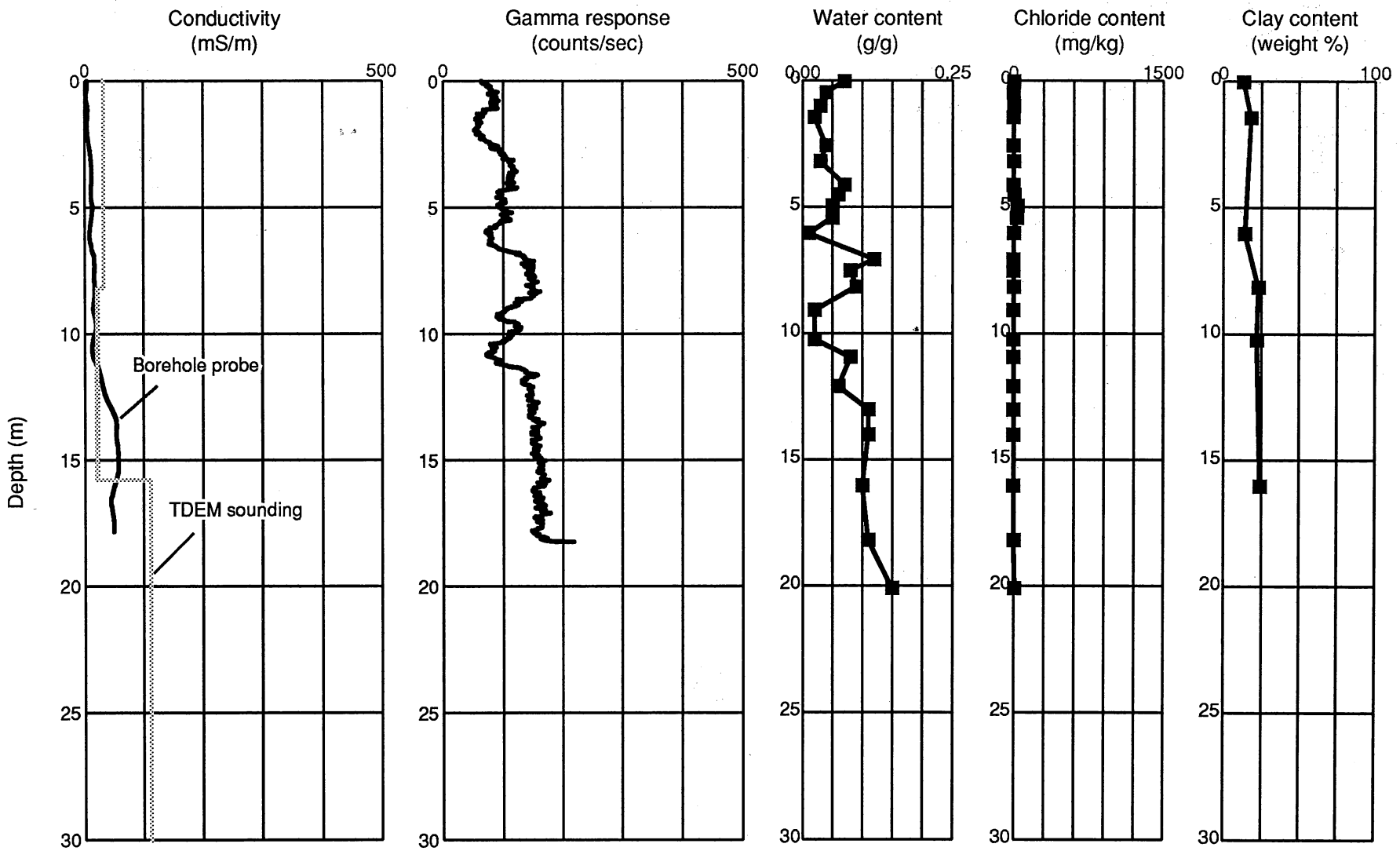

Figure 7. Conductivity, gamma response, soil water content (per gram of sample), chloride content (per kilogram of sample), and clay content for borehole RLB 0m at the Red Light Bolson fissure.

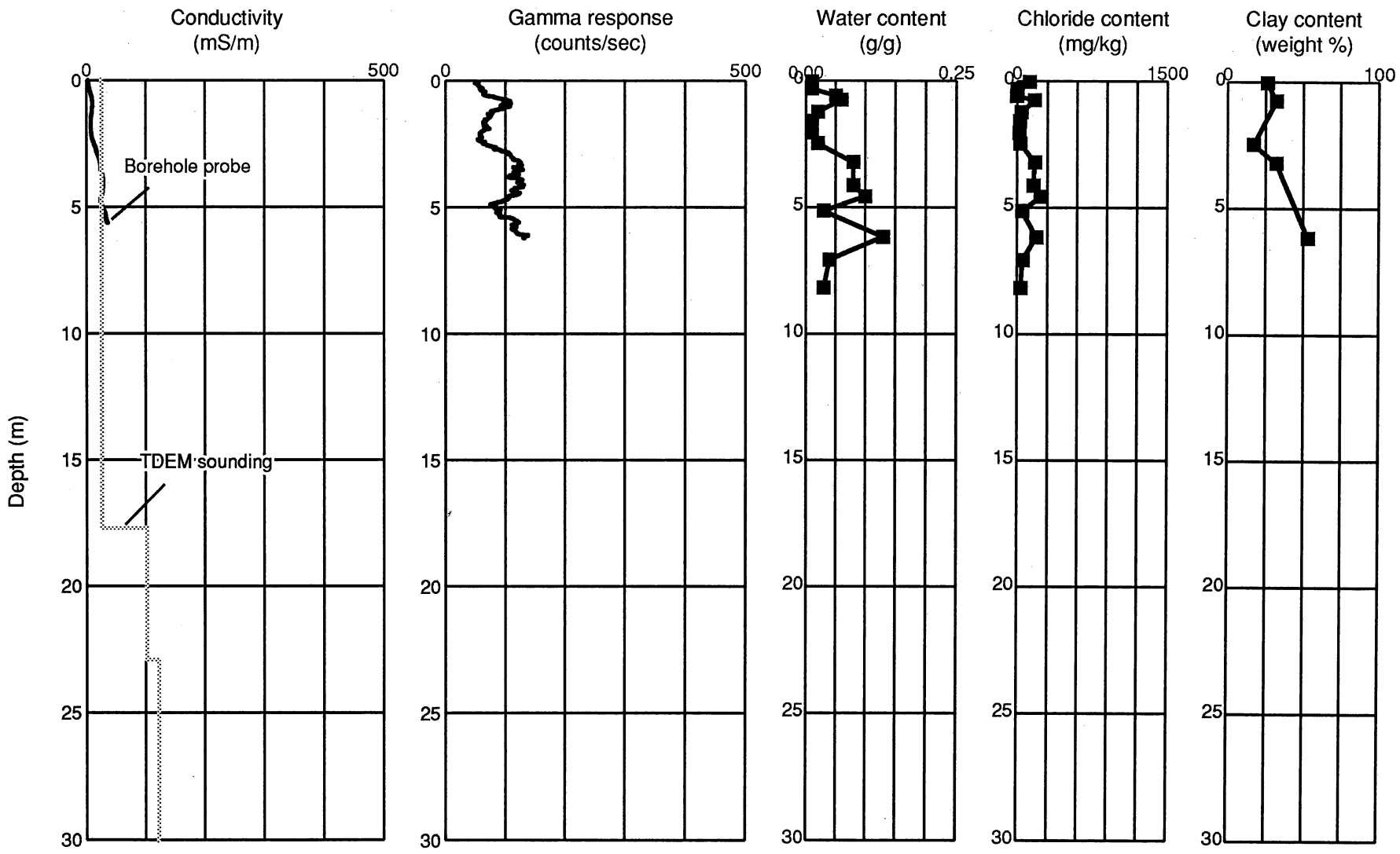

Figure 8. Conductivity, gamma response, soil water content (per gram of sample), chloride content (per kilogram of sample), and clay content for borehole RLB 50m at the Red Light Bolson fissure.

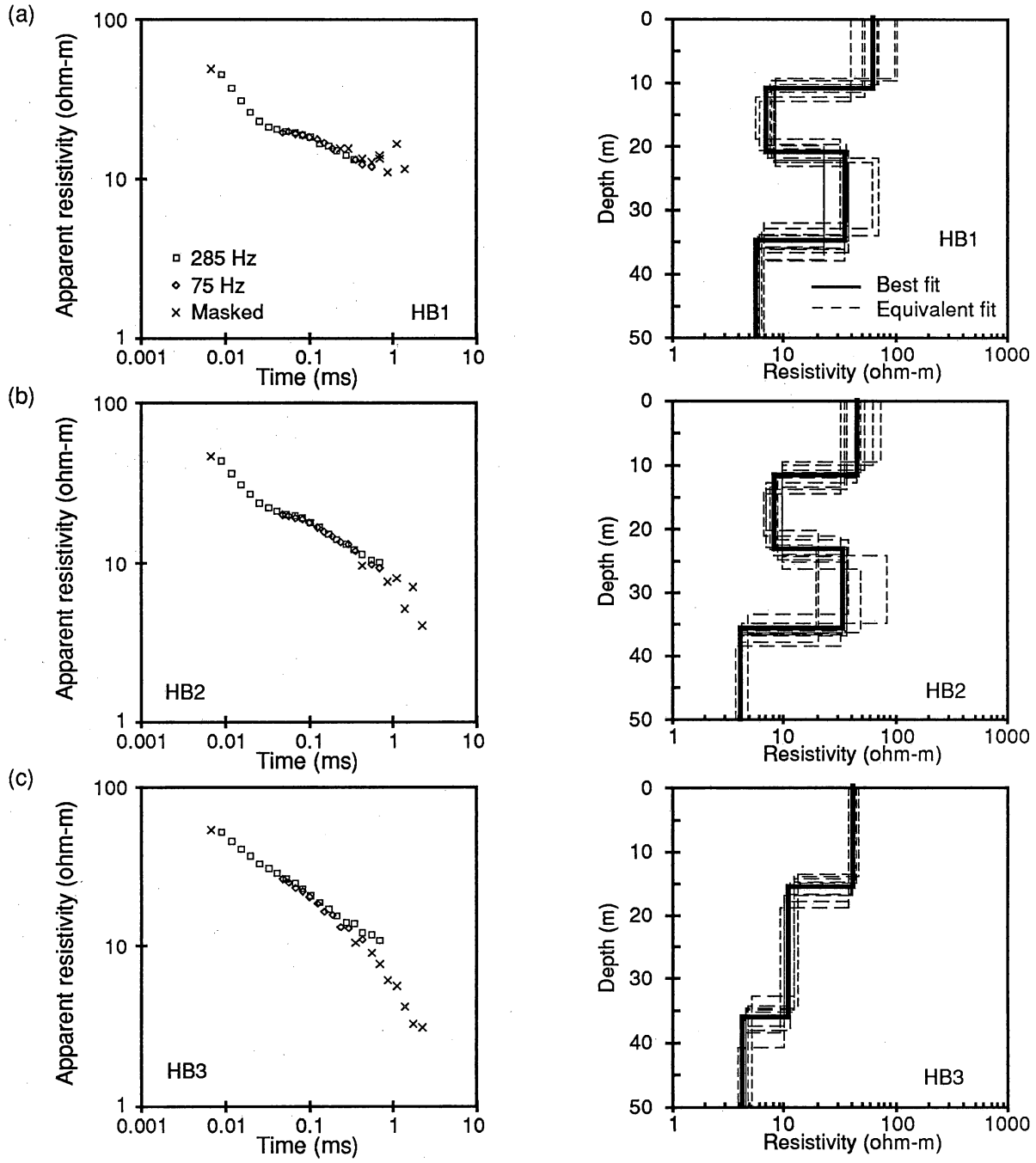

Figure 9. Transient decays (left) and best-fit vertical resistivity models (right) for time-domain soundings in the Hueco Bolson area. Sounding HB1 (a) is located at borehole HBF 0m at the center of a fissure, sounding HB2 (b) is located 10 m south of the fissure at borehole HBF 10m, and sounding HB3 (c) is located 50 m south of the fissure at borehole HBF 50m. Location shown in fig. 1.

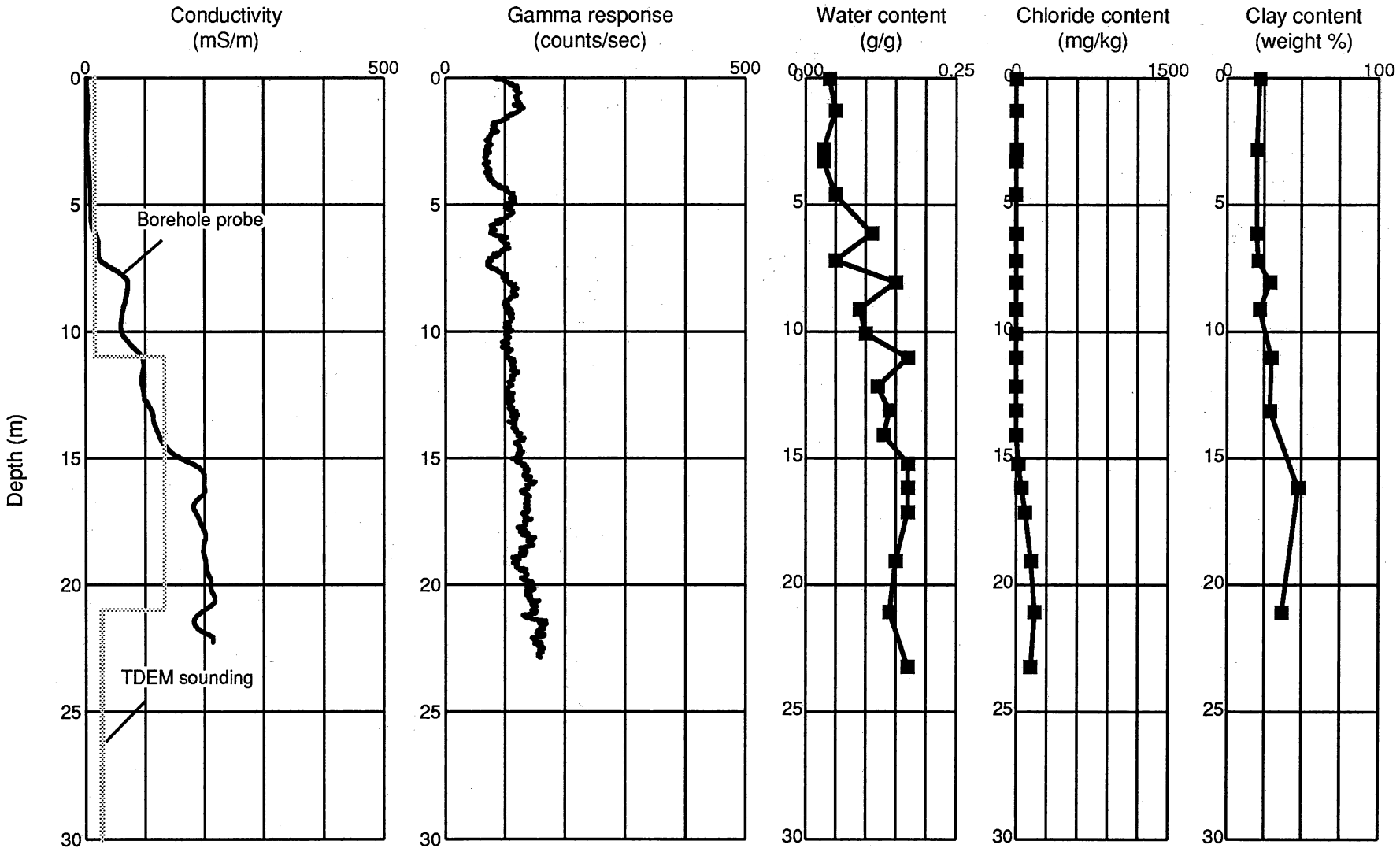

Figure 10. Conductivity, gamma response, soil water content (per gram of sample), chloride content (per kilogram of sample), and clay content for borehole HBF 0m at the Hueco Bolson fissure.

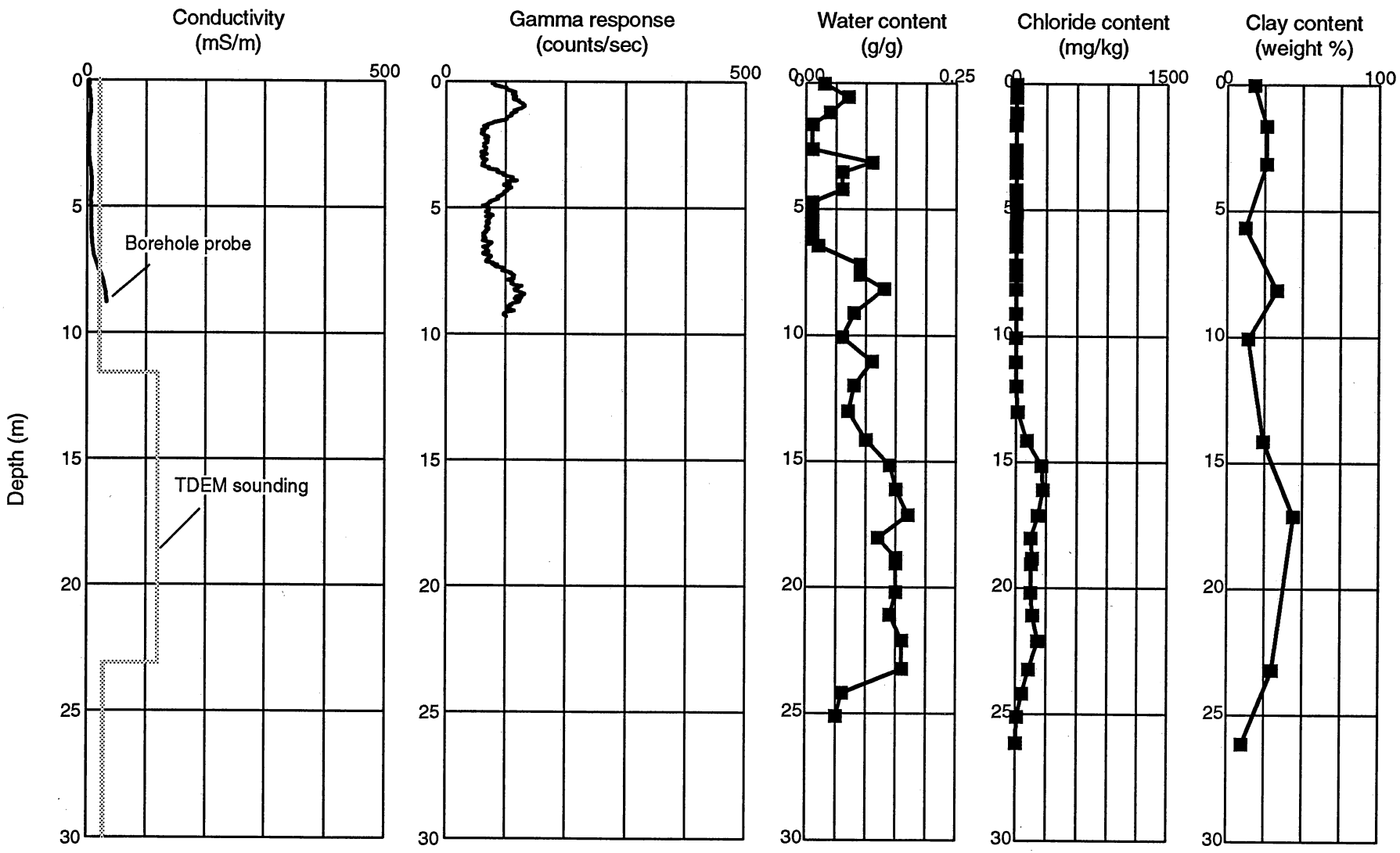

Figure 11. Conductivity, gamma response, soil water content (per gram of sample), chloride content (per kilogram of sample), and clay content for borehole HBF 10m at the Hueco Bolson fissure.

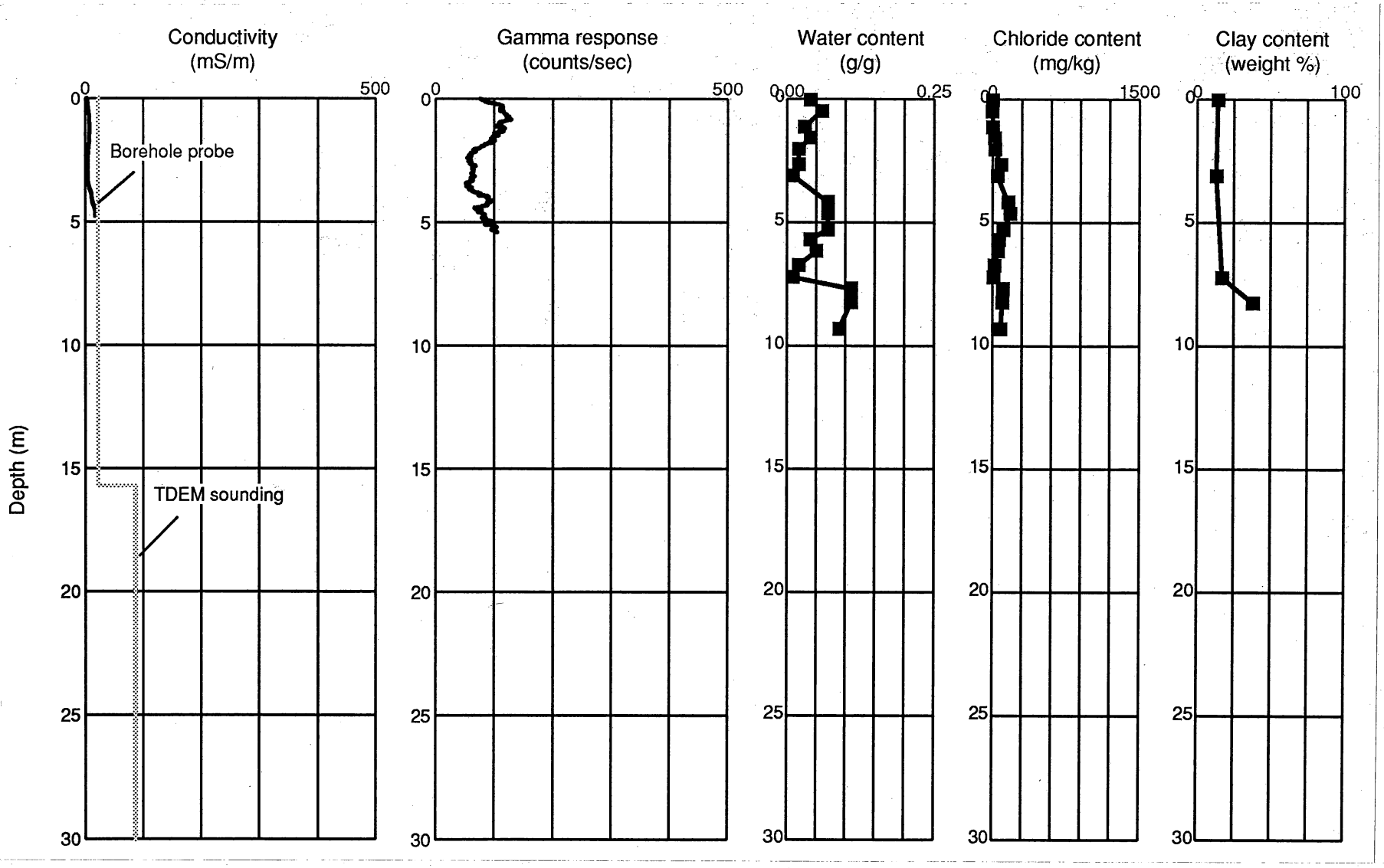

Figure 12. Conductivity, gamma response, soil water content (per gram of sample), chloride content (per kilogram of sample), and clay content for borehole HBF 50m at the Hueco Bolson fissure.

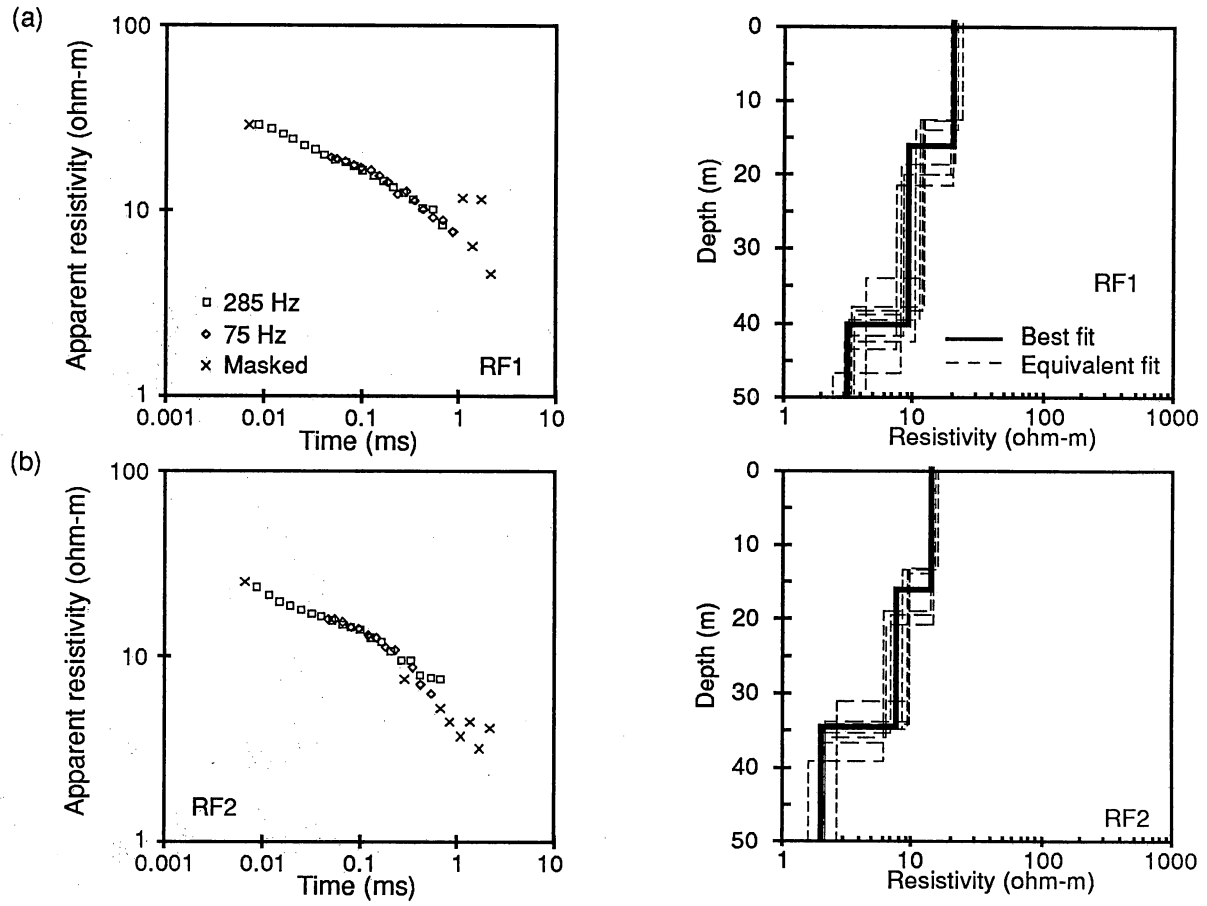

Figure 13. Transient decays (left) and best-fit vertical resistivity models (right) for time-domain soundings at the Ryan Flat fissure near Valentine, Texas. Sounding RF1 (a) is located at borehole RFF 50m about 50 m northeast of the fissure and sounding RF2 (b) is located at borehole RFF 10m about 10 m northeast of the fissure. Location shown in fig. 1.

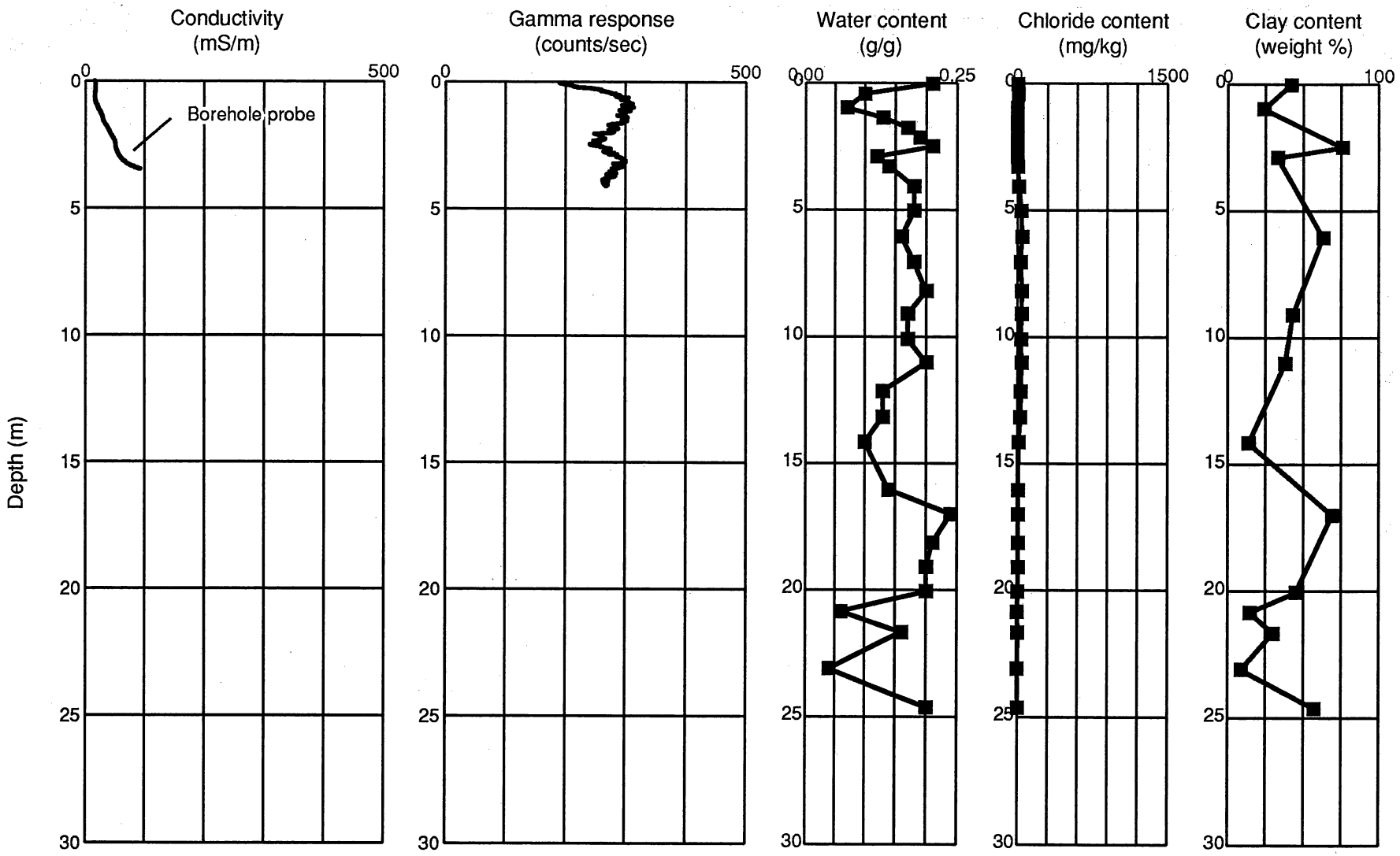

Figure 14. Conductivity, gamma response, soil water content (per gram of sample), chloride content (per kilogram of sample), and clay content for borehole RFF 0m at the Ryan Flat fissure.

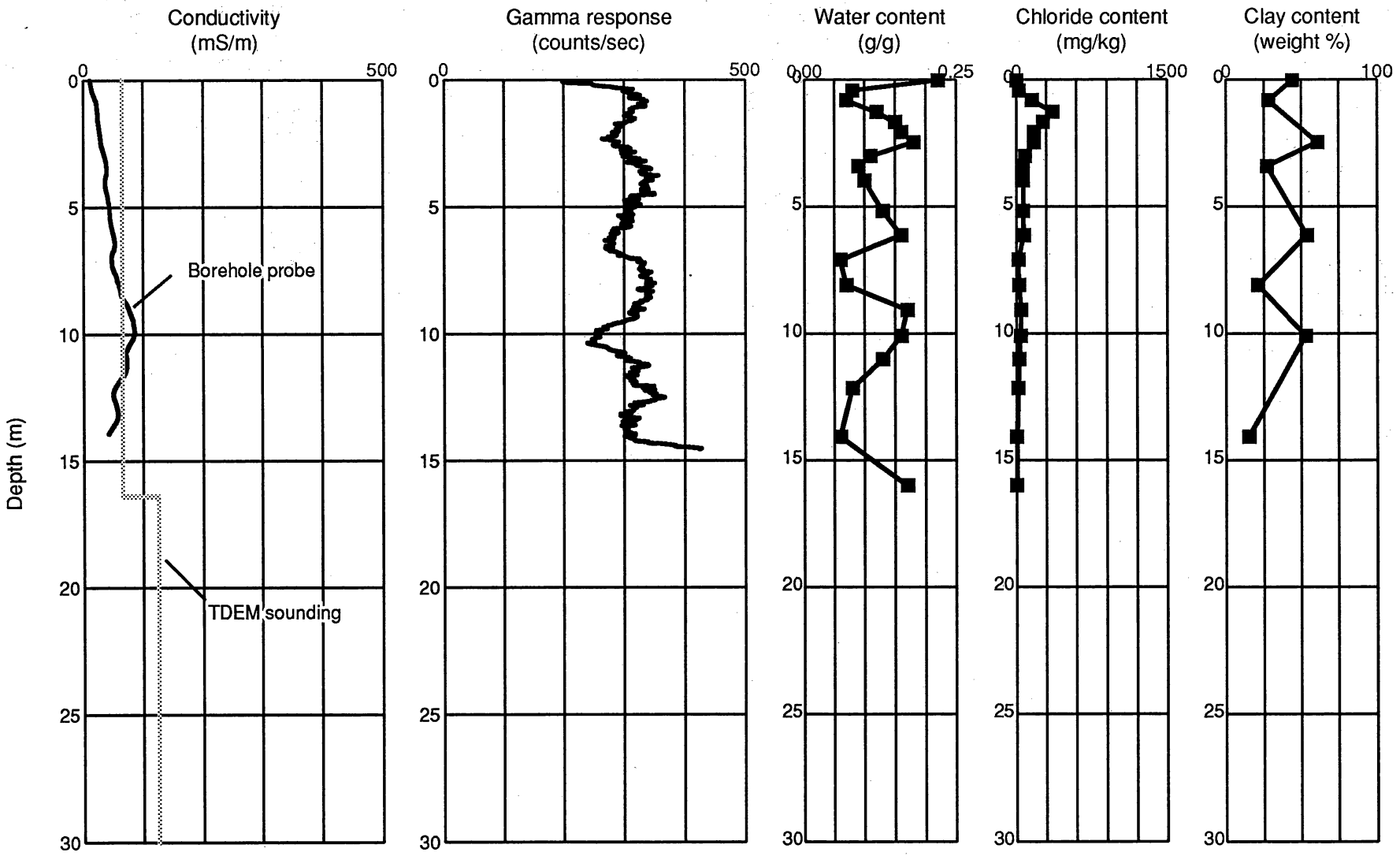

Figure 15. Conductivity, gamma response, soil water content (per gram of sample), chloride content (per kilogram of sample), and clay content for borehole RFF 10m at Ryan Flat.

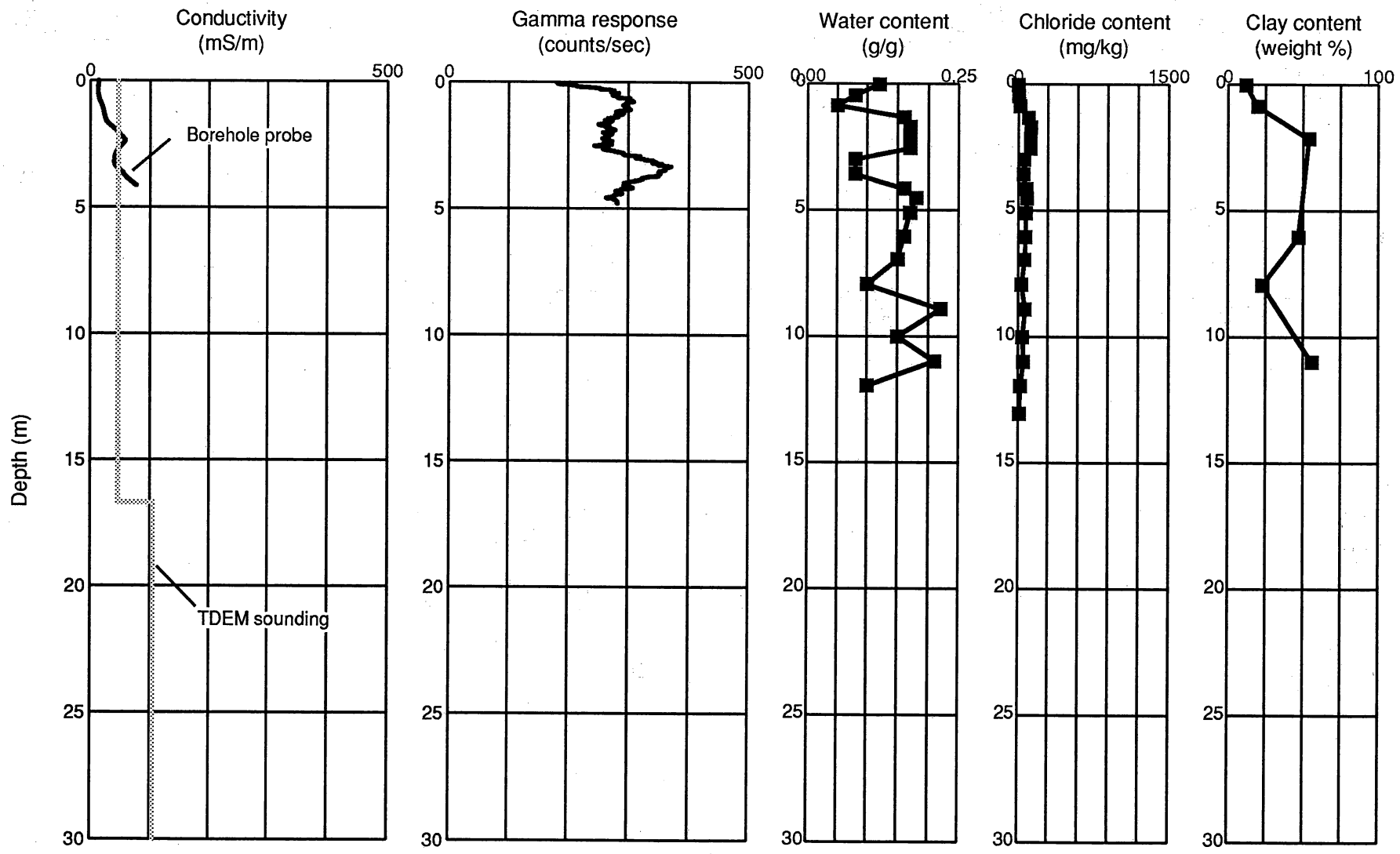

Figure 16. Conductivity, gamma response, soil water content (per gram of sample), chloride content (per kilogram of sample), and clay content for borehole RFF 50m at Ryan Flat.

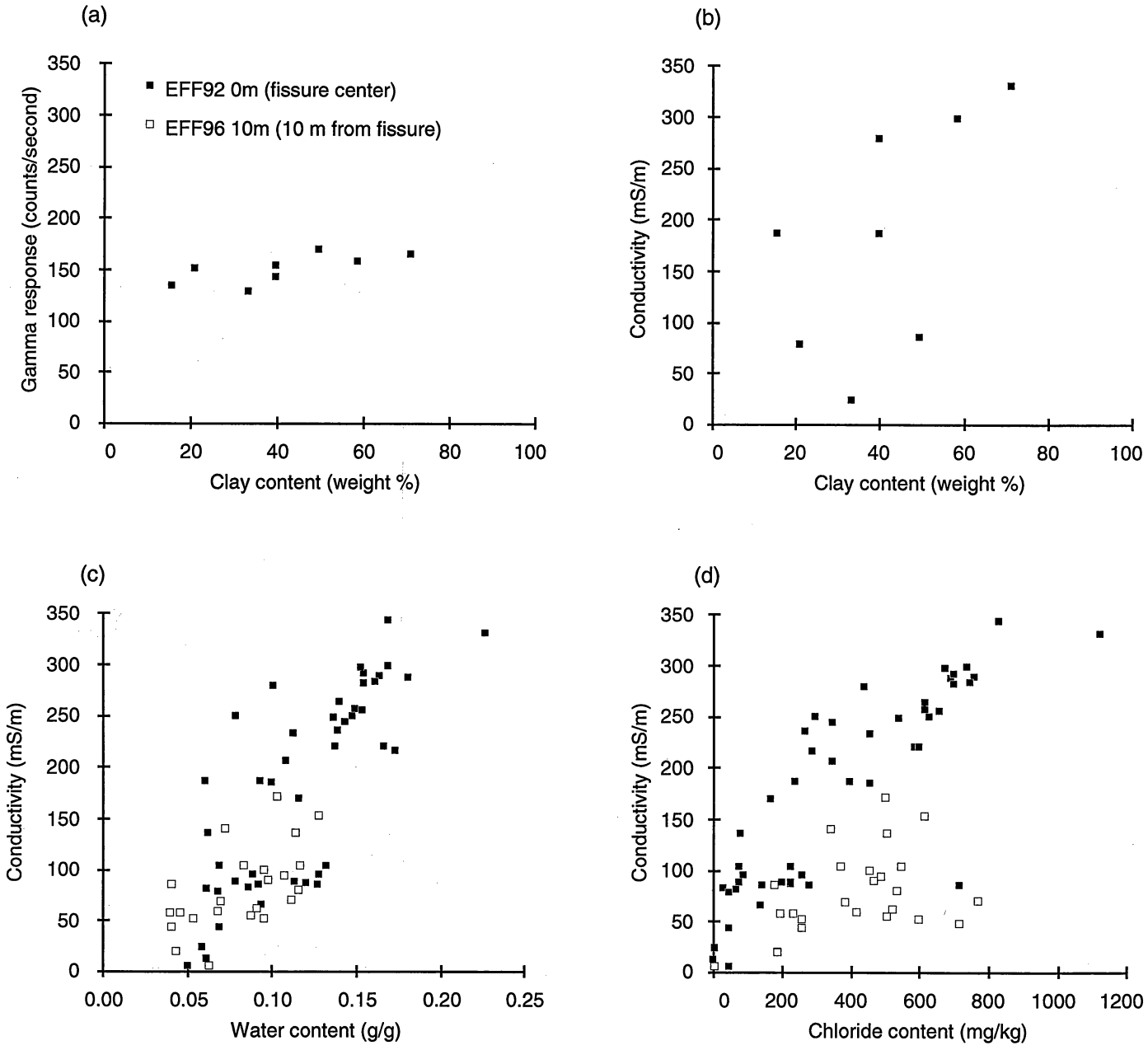

Figure 17. Relationships between (a) gamma response and clay content, (b) conductivity and clay content, (c) conductivity and water content, and (d) conductivity and chloride content at Eagle Flat boreholes EFF92 0m at the center of the fissure and EFF96 10m east of the fissure.

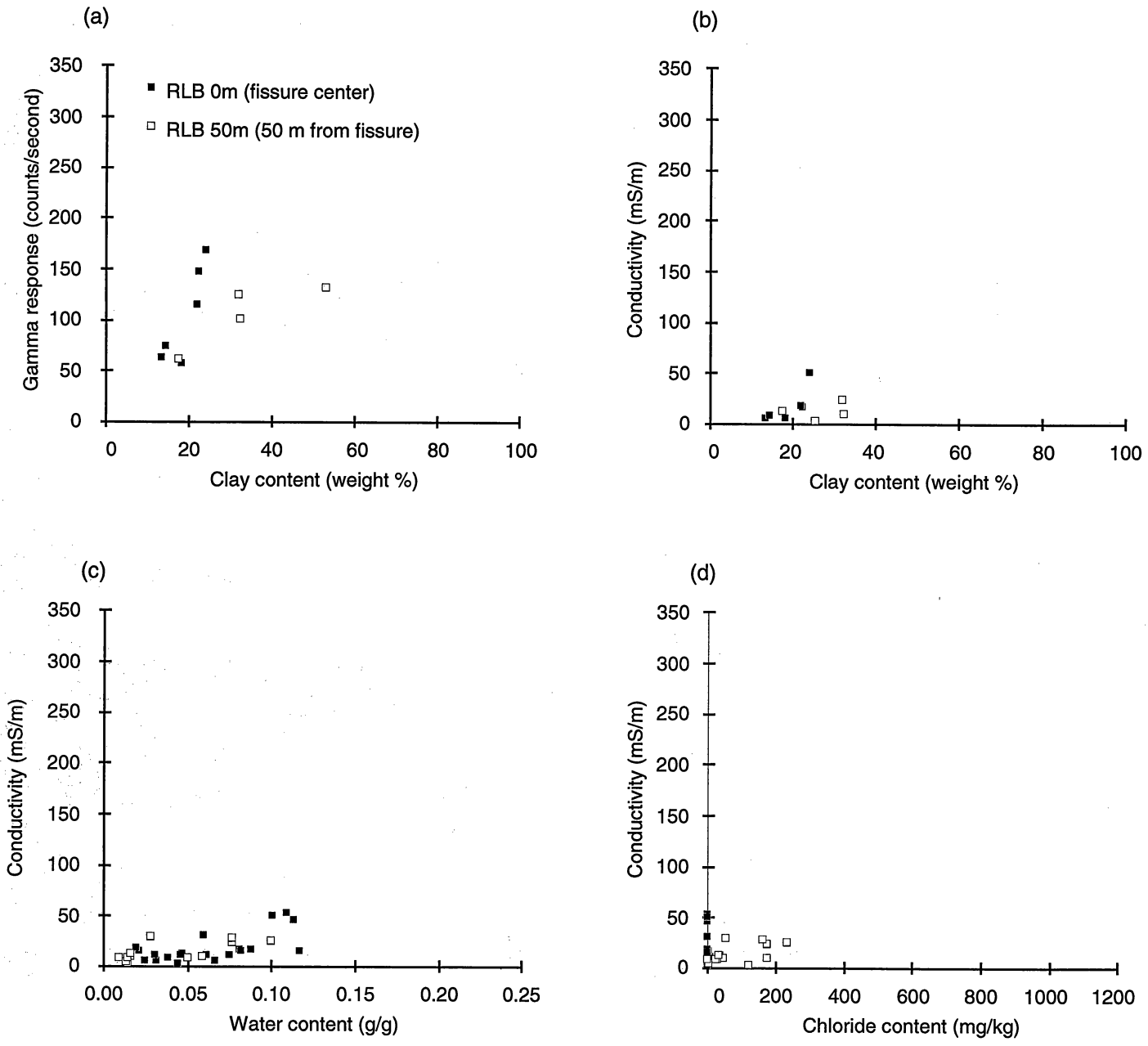

Figure 18. Relationships between (a) gamma response and clay content, (b) conductivity and clay content, (c) conductivity and water content, and (d) conductivity and chloride content at Red Light Bolson boreholes RLB 0m at the center of the fissure and RLB 50 m east of the fissure.

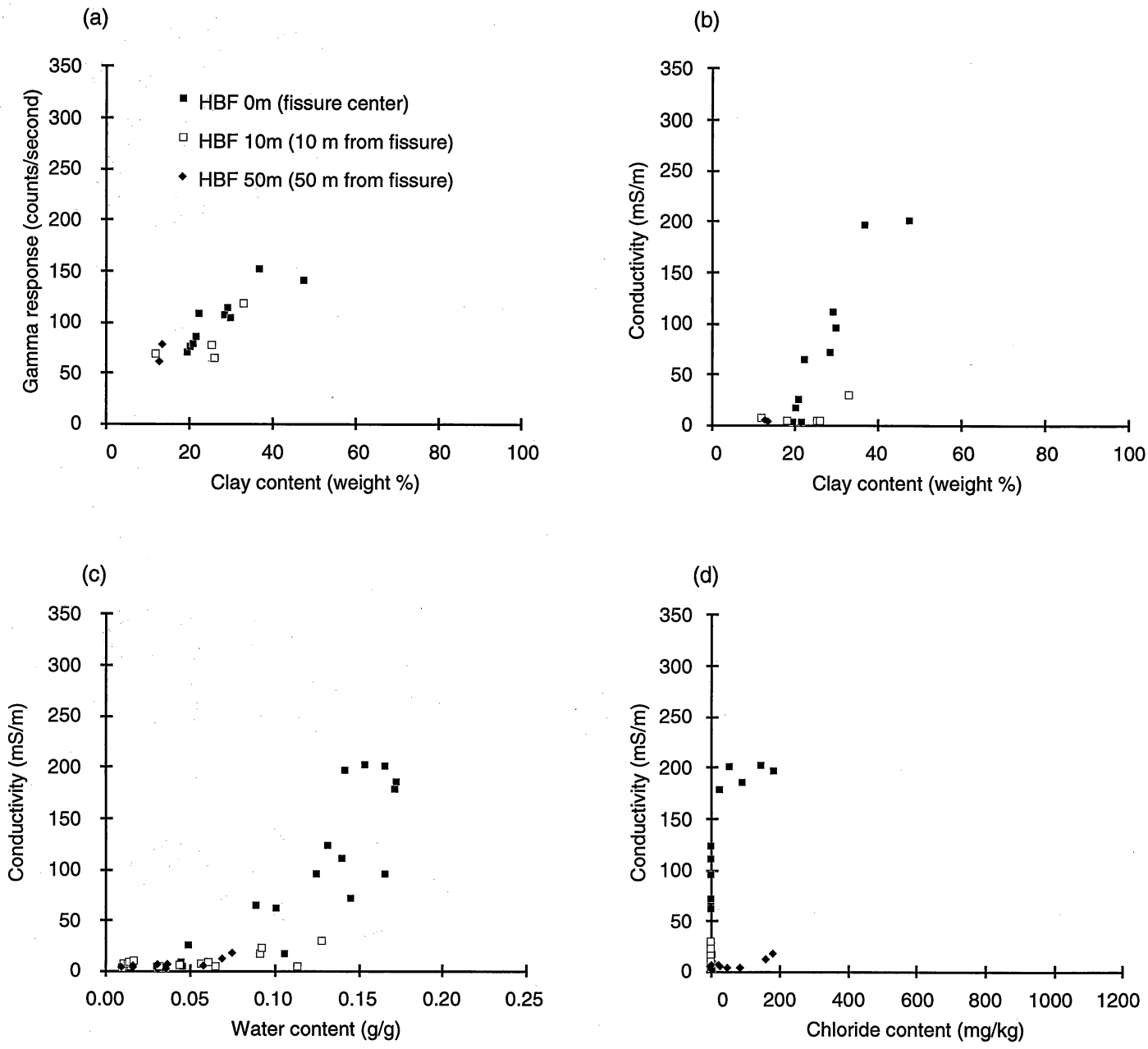

Figure 19. Relationships between (a) gamma response and clay content, (b) conductivity and clay content, (c) conductivity and water content, and (d) conductivity and chloride content at Hueco Bolson boreholes HBF 0m at the center of the fissure, HBF 10 m south of the fissure, and HBF 50 m south of the fissure.

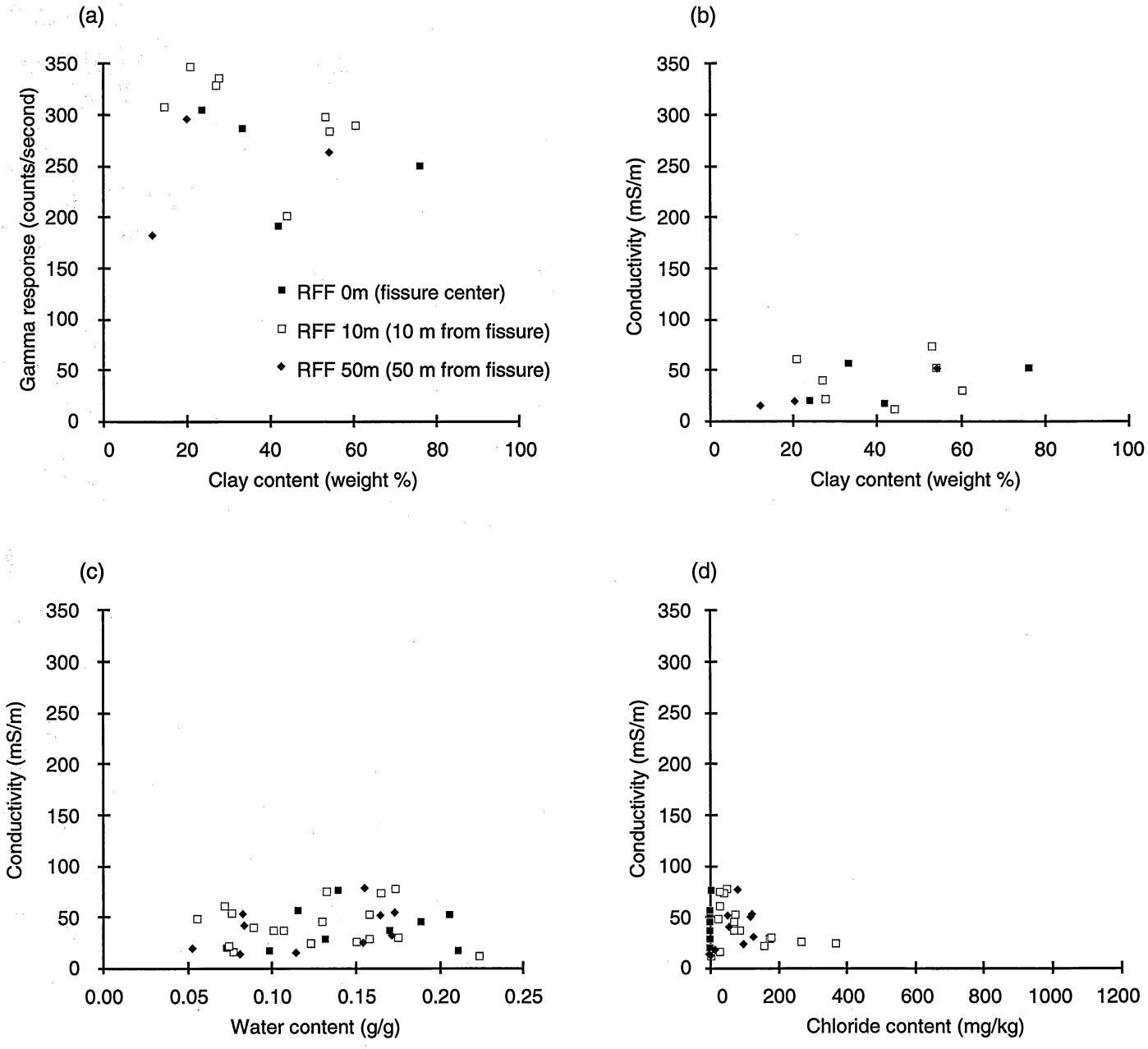

Figure 20. Relationships between (a) gamma response and clay content, (b) conductivity and clay content, (c) conductivity and water content, and (d) conductivity and chloride content at Ryan Flat boreholes RFF 0m at the center of the fissure, RFF 10 m northeast of the fissure, and RFF 50 m northeast of the fissure.

Table 1. Location, borehole name, depth logged, and date logged for conductivity and gamma ray logs of boreholes in the Eagle Flat, Red Light Bolson, Hueco Bolson, and Ryan Flat fissure areas.

Location	Borehole	Depth logged (m)	Date logged
Eagle Flat			
Eagle Flat fissure (center)	EFF92 0m	22	9/12/94
Eagle Flat fissure (flank, 10 m east)	EFF96 10m	14	9/12/94
Red Light Bolson			
Red Light Bolson fissure (center)	RLB 0m	18	9/13/94
Red Light Bolson fissure (flank, 50 m east)	RLB 50m	6	9/13/94
Hueco Bolson			
Hueco Bolson fissure (center)	HBF 0m	22	9/14/94
Hueco Bolson fissure (flank, 10 m south)	HBF 10m	9	9/14/94
Hueco Bolson fissure (flank, 50 m south)	HBF 50m	5	9/14/94
Ryan Flat			
Ryan Flat fissure (center)	RFF 0m	4	9/14/94
Ryan Flat fissure (flank, 10 m north)	RFF 10m	14	9/14/94
Ryan Flat fissure (flank, 50 m north)	RFF 50m	4	9/14/94

Table 2. Best-fit resistivity models for time-domain electromagnetic soundings in the Eagle Flat, Red Light Bolson, Hueco Bolson, and Ryan Flat fissure areas.

Sounding	Resistivity (ohm-m)	Conductivity (mS/m)	Layer thickness (m)	Depth to top (m)	Fitting error (%)
Eagle Flat					
Sounding EF1 at Eagle Flat fissure center, borehole EFF92 0m					3.5
Layer 1	104.7	10	7.0	0.0	
Layer 2	5.2	194	14.6	7.0	
Layer 3	3.5	282		21.7	
Sounding EF2 at Eagle Flat fissure flank, borehole EFF96 10m					4.0
Layer 1	11.1	90	14.8	0.0	
Layer 2	4.2	240	14.0	14.8	
Layer 3	2.7	370		28.8	
Sounding EF3, 30 m east of Eagle Flat fissure					4.5
Layer 1	15.4	65	13.8	0.0	
Layer 2	4.7	214		13.8	
Sounding EF4, 30 m west of Eagle Flat fissure					2.8
Layer 1	15.0	67	9.2	0.0	
Layer 2	7.7	130	10.4	9.2	
Layer 3	3.2	310		19.6	
Red Light Bolson					
Sounding RLB1 at Red Light Bolson fissure center, borehole RLB 0m					4.3
Layer 1	30.8	32	8.2	0.0	
Layer 2	47.1	21	7.6	8.2	
Layer 3	8.8	113		15.8	
Sounding RLB2 at Red Light Bolson fissure flank, borehole RLB 50m					5.7
Layer 1	39.8	25	17.7	0.0	
Layer 2	9.8	102	5.1	17.7	
Layer 3	8.2	122		22.9	
Hueco Bolson					
Sounding HB1 at Hueco Bolson fissure center, borehole HBF 0m					3.0
Layer 1	65.7	15	11.0	0.0	
Layer 2	7.5	133	10.0	11.0	
Layer 3	37.1	27	14.0	21.0	
Layer 4	6.1	163		35.0	
Sounding HB2 at Hueco Bolson fissure flank, borehole HBF 10m					3.4
Layer 1	46.2	22	11.6	0.0	
Layer 2	8.3	120	11.5	11.6	
Layer 3	34.3	29	12.6	23.1	
Layer 4	4.1	242		35.7	
Sounding HB3 at Hueco Bolson fissure flank, borehole HBF 50m					3.7
Layer 1	43.5	23	15.7	0.0	
Layer 2	11.6	87	20.5	15.7	
Layer 3	4.6	217		36.3	

Ryan Flat

Sounding RF1 at Ryan Flat fissure flank (50 m northeast), borehole RFF 50m					6.2
Layer 1	21.3	47	16.7	0.0	
Layer 2	9.6	105	23.9	16.7	
Layer 3	3.2	311		40.6	
Sounding RF2 at Ryan Flat fissure flank (10 m northeast), borehole RFF 10m					4.9
Layer 1	15.2	66	16.4	0.0	
Layer 2	8.0	125	18.4	16.4	
Layer 3	2.2	463		34.8	

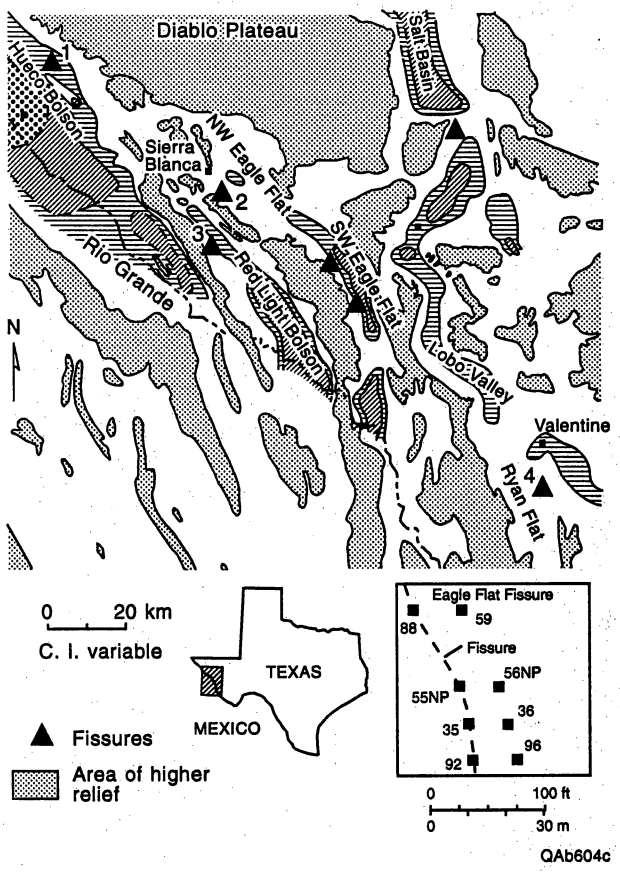

Figure 1. Map of fissures in study area: (1) Hueco Bolson, (2) Eagle Flat, (3) Red Light Bolson, and (4) Ryan Flat (modified from Baumgardner and Scanlon, 1992).

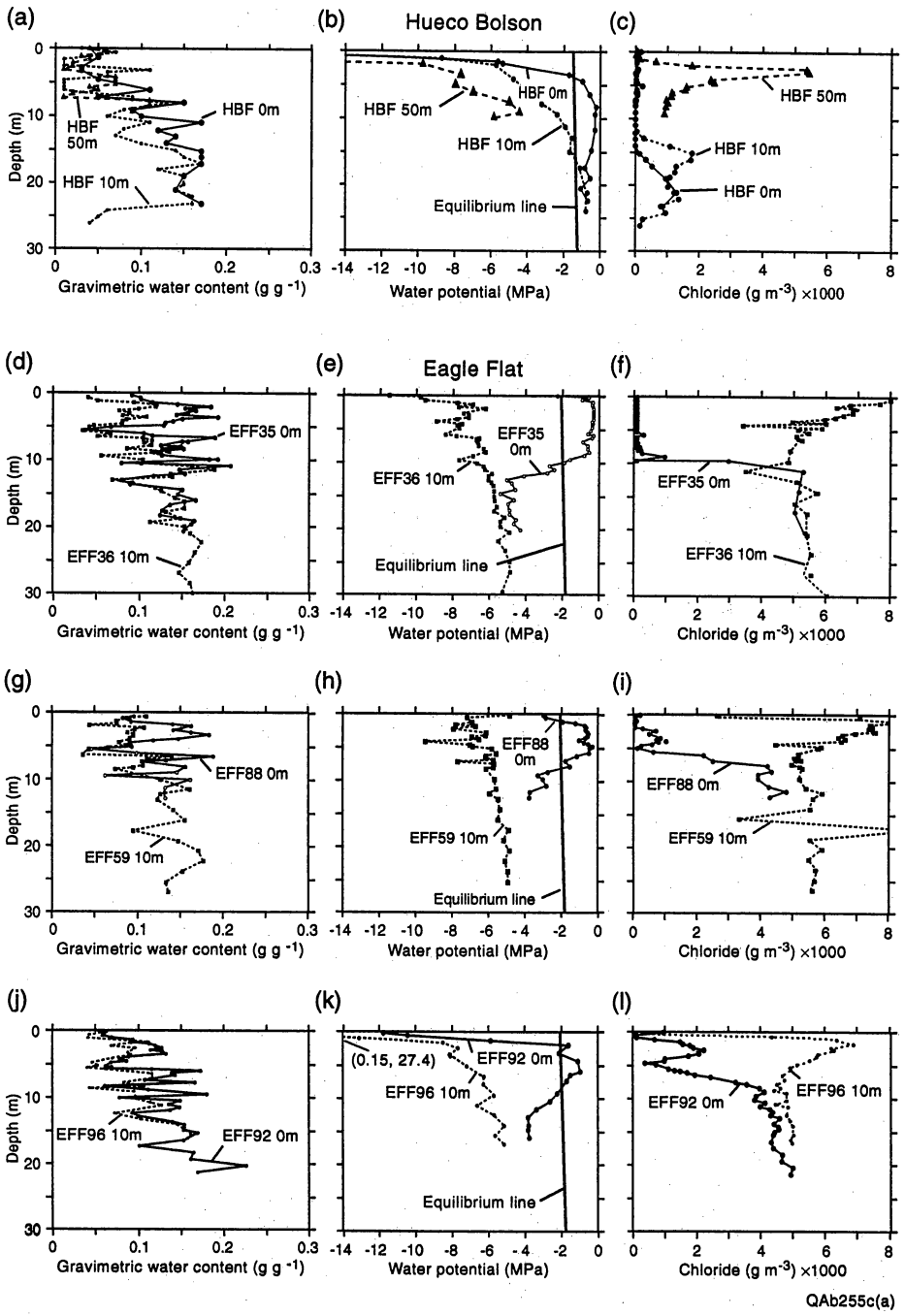

Figure 2. Profiles of texture, gravimetric water content, water potential, and chloride concentrations in and adjacent to Hueco Bolson and Eagle Flat fissures.

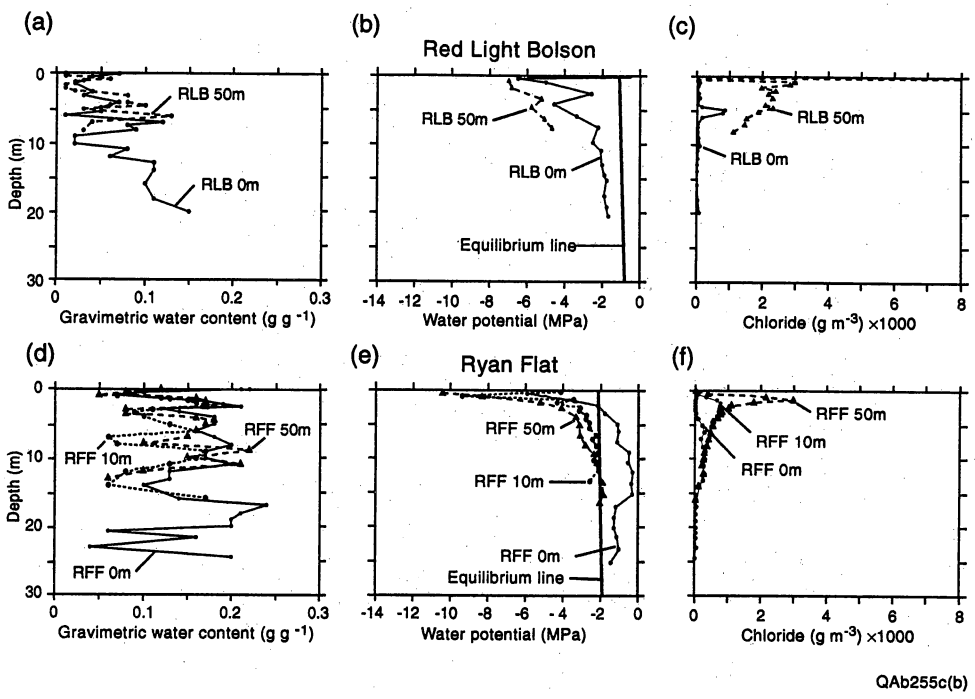

Figure 3. Profiles of texture, gravimetric water content, water potential, and chloride concentrations in and adjacent to Red Light Bolson and Ryan Flat fissures.

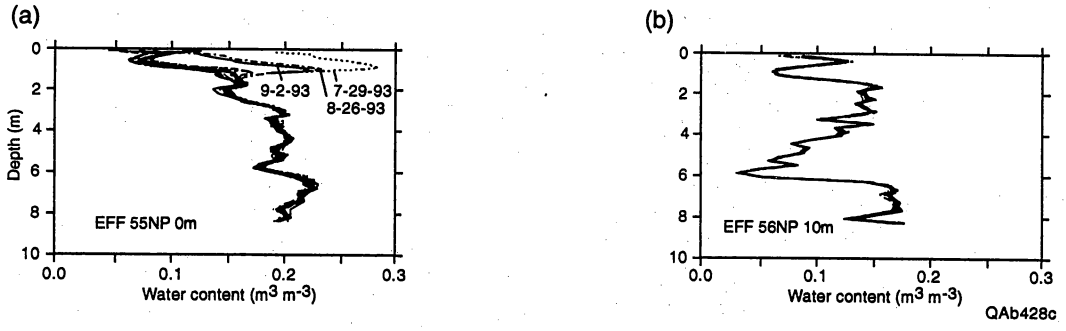

Figure 4. Variation in water content with depth and time in neutron probe access tubes in and 10 m distant from Eagle Flat fissure. Water content was monitored approximately monthly from June 1993 to August 1994 and in February and May, 1995.

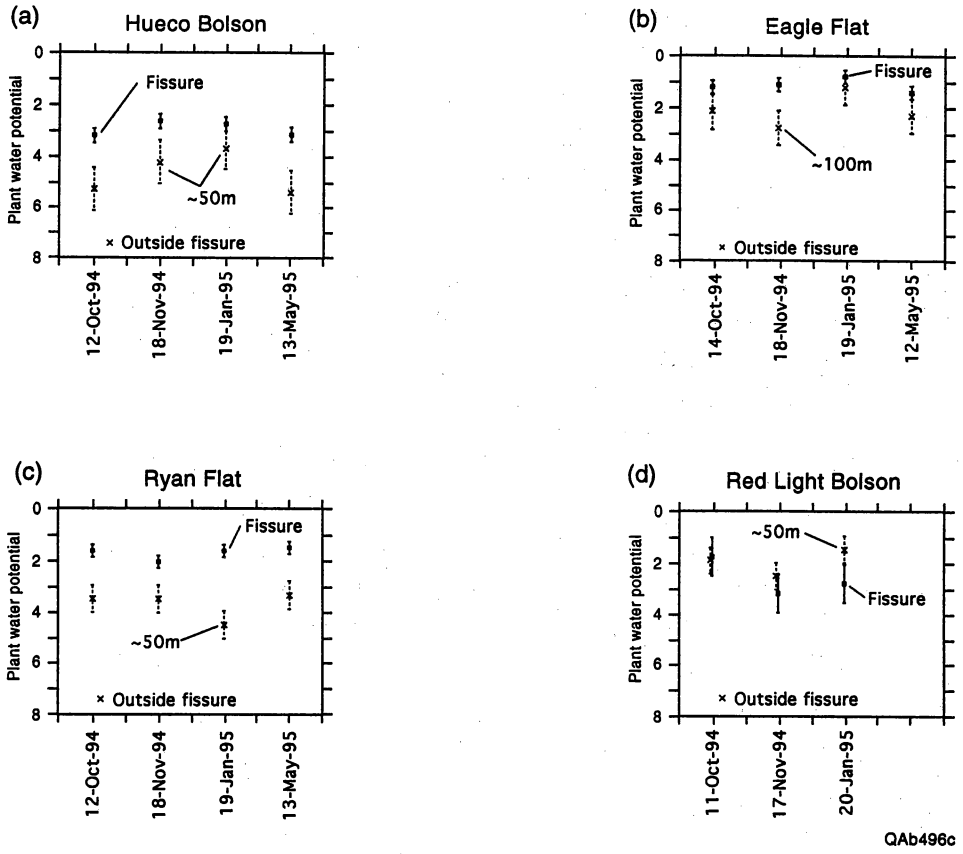

Figure 5. Predawn plant water potentials measured in and adjacent to fissures.

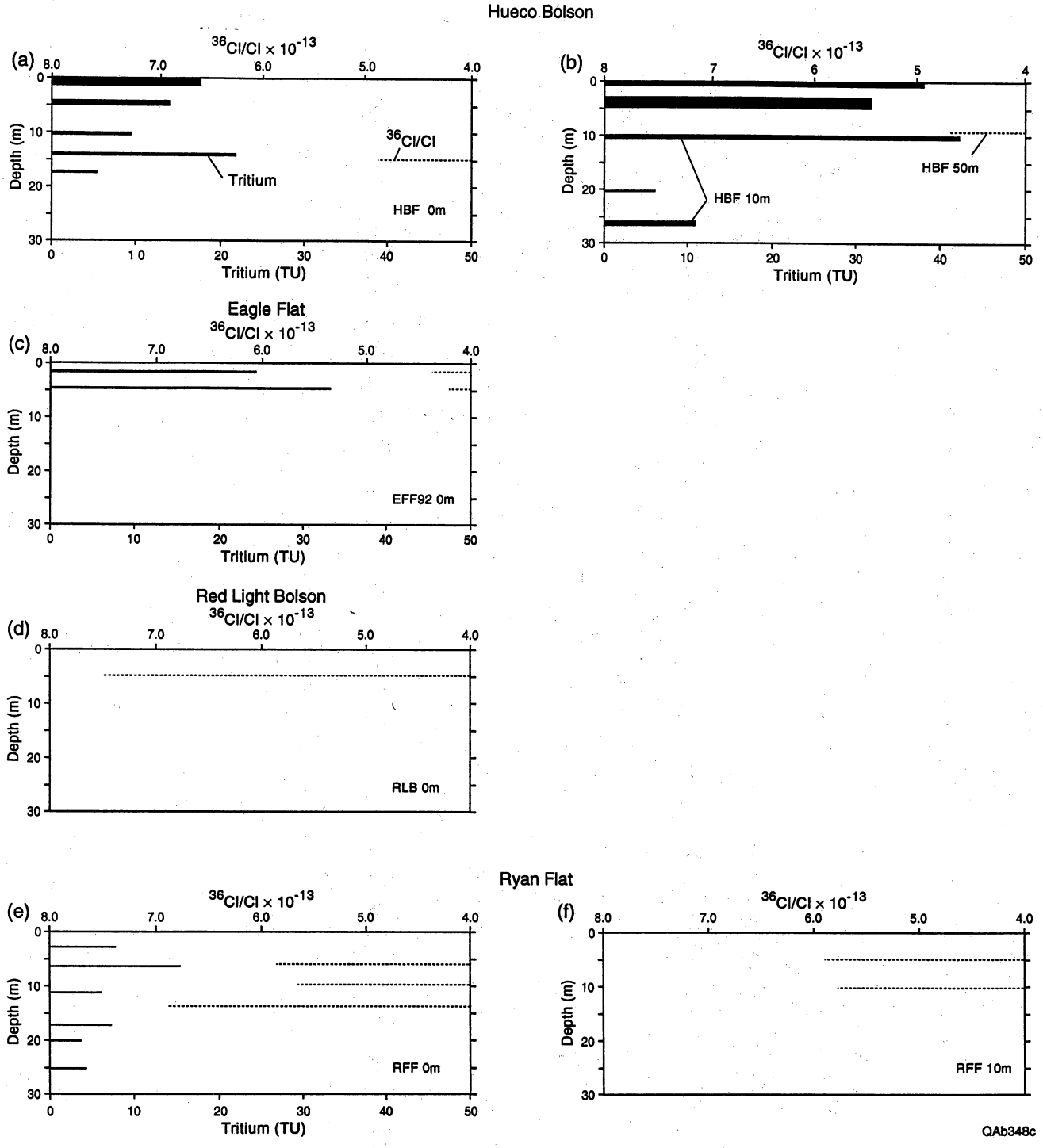

Figure 6. Variations in ^{3}H and $^{36}Cl/Cl$ in profiles in and adjacent to fissures.

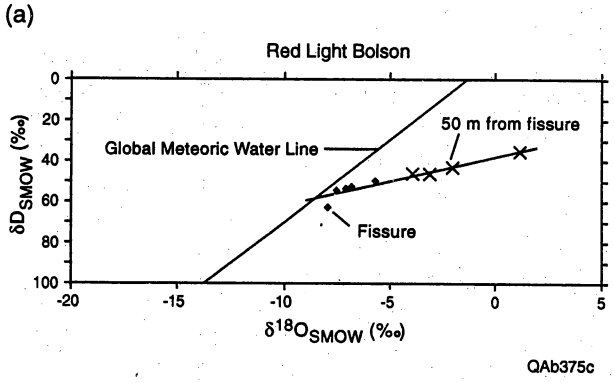

Figure 7. Stable isotopes of oxygen and hydrogen for a profile beneath Red Light Bolson fissure and 50 m distant from the fissure.

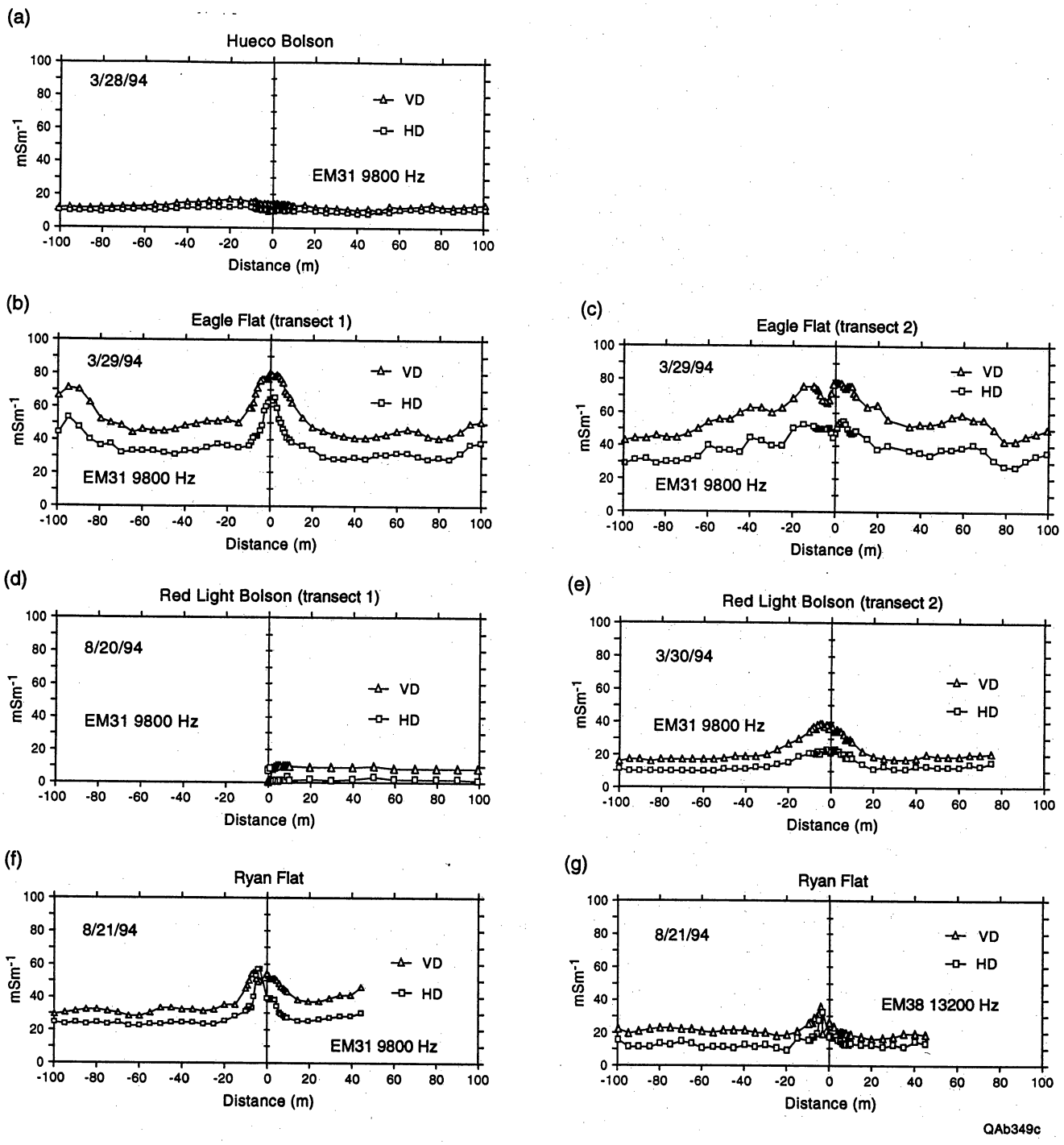

Figure 8. Electromagnetic transects across fissures.